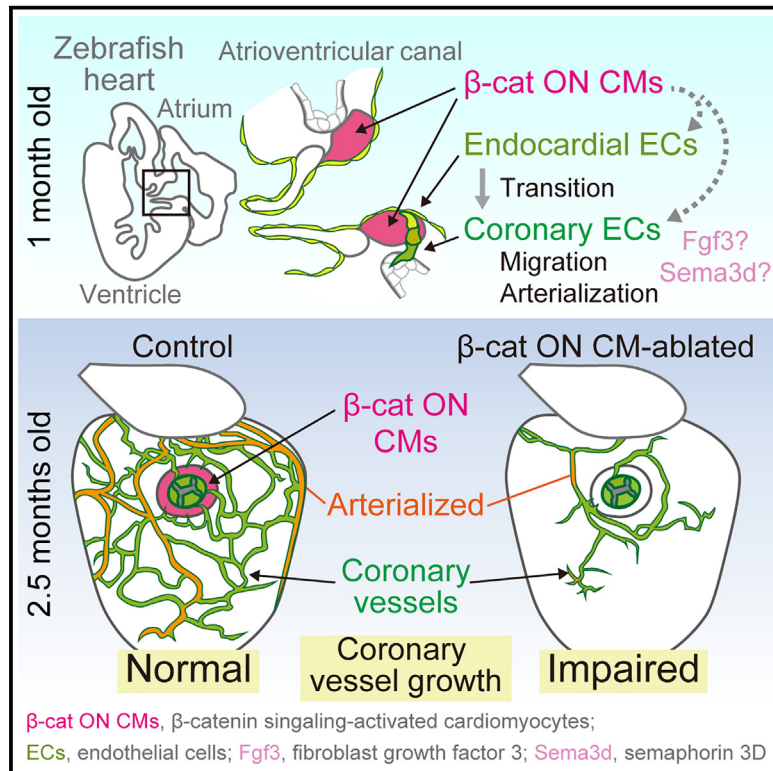


# Developmental Cell

## Zonated Wnt/ $\beta$ -catenin signal-activated cardiomyocytes at the atrioventricular canal promote coronary vessel formation in zebrafish

### Graphical abstract



### Authors

Ayano Chiba, Takuya Yamamoto, Hajime Fukui, Moe Fukumoto, Manabu Shirai, Hiroyuki Nakajima, Naoki Mochizuki

### Correspondence

achiba@med.id.yamagata-u.ac.jp (A.C.),  
mochizuki@ncvc.go.jp (N.M.)

### In brief

Chiba et al. identify a zone of cardiomyocytes (CMs) with continuous activation of Wnt/ $\beta$ -catenin signaling in zebrafish. These CMs control the transition of endocardial to coronary endothelial cells by promoting their migration and arterialization.

### Highlights

- The Wnt/ $\beta$ -catenin signaling<sup>+</sup> cardiomyocyte ( $\beta$ -cat ON CM) zone was found at the AVC
- $\beta$ -cat ON CMs at the AVC are activated by Wnt ligands from the beating heart
- Ablation of  $\beta$ -cat ON CMs results in impaired coronary vessel development
- $\beta$ -cat ON CMs control transition of endocardial to coronary endothelial cells

Short article

# Zonated Wnt/ $\beta$ -catenin signal-activated cardiomyocytes at the atrioventricular canal promote coronary vessel formation in zebrafish

Ayano Chiba,<sup>1,2,\*</sup> Takuya Yamamoto,<sup>3,4,5</sup> Hajime Fukui,<sup>1,6</sup> Moe Fukumoto,<sup>1</sup> Manabu Shirai,<sup>7</sup> Hiroyuki Nakajima,<sup>1</sup> and Naoki Mochizuki<sup>1,8,\*</sup>

<sup>1</sup>Department of Cell Biology, National Cerebral and Cardiovascular Center Research Institute, Suita, Osaka 564-8565, Japan

<sup>2</sup>Department of Pharmacology, Yamagata University School of Medicine, Yamagata 990-9585, Japan

<sup>3</sup>Department of Life Science Frontiers, Center for iPS Cell Research and Application (CiRA), Kyoto University, Kyoto 606-8507, Japan

<sup>4</sup>Institute for the Advanced Study of Human Biology (WPI-ASHBi), Kyoto University, Yoshida-Konoe-cho, Sakyo-ku, Kyoto 606-8501, Japan

<sup>5</sup>Medical-Risk Avoidance Based on iPS Cells Team, RIKEN Center for Advanced Intelligence Project (AIP), Kyoto 606-8507, Japan

<sup>6</sup>Division of Biomechanics and Signaling, Institute of Advanced Medical Sciences, Tokushima University, Tokushima 770-8503, Japan

<sup>7</sup>Omics Research Center, National Cerebral and Cardiovascular Center, Suita, Osaka 564-8565, Japan

<sup>8</sup>Lead contact

\*Correspondence: [achiba@med.id.yamagata-u.ac.jp](mailto:achiba@med.id.yamagata-u.ac.jp) (A.C.), [mochizuki@ncvc.go.jp](mailto:mochizuki@ncvc.go.jp) (N.M.)

<https://doi.org/10.1016/j.devcel.2024.09.012>

## SUMMARY

Cells functioning at a specific zone by clustering according to gene expression are recognized as zonated cells. Here, we demonstrate anatomical and functional zones in the zebrafish heart. The cardiomyocytes (CMs) at the atrioventricular canal between the atrium and ventricle could be grouped into three zones according to the localization of signal-activated CMs: Wnt/ $\beta$ -catenin signal<sup>+</sup>, Bmp signal<sup>+</sup>, and Tbx2b<sup>+</sup> zones. Endocardial endothelial cells (ECs) changed their characteristics, penetrated the Wnt/ $\beta$ -catenin signal<sup>+</sup> CM zone, and became coronary ECs covering the heart. Coronary vessel length was reduced when the Wnt/ $\beta$ -catenin signal<sup>+</sup> CMs were depleted. Collectively, we demonstrate the importance of anatomical and functional zonation of CMs in the zebrafish heart.

## INTRODUCTION

The heart functions as a pump constituted by the myocardium, endocardium, epicardium, and coronary vessels (CVs). To maintain heart function, cardiomyocytes (CMs) require complex regional differences in metabolic activity, electrophysiology, and cell coupling.<sup>1</sup> Recent technology, such as single-cell RNA sequencing (scRNA-seq), has identified detailed cellular heterogeneity and spatial transcriptomic profiling.<sup>2,3</sup> Cellular functional changes along an anatomical axis are called “zonation.”<sup>4</sup> The zonated gene expression in the heart is disturbed by congenital cardiomyopathy, suggesting that zonation is essential for heart function.<sup>2</sup> However, the function of each zone of CMs is not well understood.

Wnt/ $\beta$ -catenin signaling regulates diverse cellular functions during embryogenesis. The binding of Wnt ligands to the receptor complex of frizzled and low-density lipoprotein receptor-related protein 5/6 results in the nuclear translocation of stabilized  $\beta$ -catenin. In the nucleus,  $\beta$ -catenin binds to transcription factors such as T cell factor (TCF) and promotes the expression of Wnt target genes.<sup>5</sup> During cardiogenesis, Wnt/ $\beta$ -catenin signaling is active at the atrioventricular canal (AVC) region that connects the atrium and ventricle.<sup>6</sup> Wnt/ $\beta$ -catenin signaling at the AVC is required for the formation of atrioventricular (AV)

valve<sup>6</sup> and the programming of slow-conducting AVC CMs.<sup>7</sup> However, the physiological role of Wnt/ $\beta$ -catenin signaling in the heart after embryogenesis is poorly understood.

In zebrafish, CVs originate from AVC endocardial endothelial cells (endoECs). In 1-month-old zebrafish, endoECs at the AVC penetrated the myocardium and spread to the surface of the ventricle to give rise to coronary ECs (coECs).<sup>8</sup> In mice, coECs originate from both endoECs and sinus venosus ECs.<sup>9,10</sup> It is still unclear how AVC endoECs come out from the innermost side of the heart.

In this study, we aimed to characterize zonated CMs at the AVC and demonstrated that Wnt/ $\beta$ -catenin signal-activated CMs are required for the characteristic changes of endoECs into coEC.

## RESULTS

### Wnt/ $\beta$ -catenin signaling is continuously activated at the AVC

The Wnt/ $\beta$ -catenin signaling is a key regulator of zonation in the liver and adrenal gland.<sup>11–13</sup> To examine whether Wnt/ $\beta$ -catenin signal-activated ( $\beta$ -cat ON) cells are present in other organs besides these two organs, we established a transgenic (Tg) zebrafish line: *Tg(actb2:GAL4db-TCF $\Delta$ C-2A-mCherry);Tg(UAS:EGFP)* in

which nuclear-translocated  $\beta$ -catenin induces GAL4/upstream activating sequence (UAS) system-driven EGFP expression (Figure S1A).<sup>14</sup> The general  $\beta$ -cat ON reporter was developed using the ubiquitous  $\beta$ -actin (*actb2*) promoter. EGFP was widely observed at 24 and 48 h post-fertilization (hpf), as reported previously<sup>15,16</sup>; however, most of the signals disappeared by 72 hpf except the pectoral fin, aortic arch, and AVC (Figures 1A, S1B, and S1C). We observed that  $\beta$ -cat ON cells were still present in the AVC CMs of the 3-month-old adult heart (Figure 1A).

To characterize  $\beta$ -cat ON CMs at the AVC, we developed a CM-specific  $\beta$ -cat ON reporter, *Tg(myf7:GAL4db-TCF $\Delta$ C-2A-mCherry);Tg(UAS:EGFP)*, using CM-specific myosin light chain (*myf7*) promoter. EGFP was continuously observed at the AVC from 48 hpf to adulthood, especially in the atrial CMs of the AVC (Figures 1B and 1C; Videos S1A and S1B). Reliability of the reporter was confirmed by a decrease of reporter activity in the reporter fish treated with Wnt/ $\beta$ -catenin signaling inhibitor, IWR-1-endo (IWR1),<sup>17</sup> or Wnt secretion inhibitor, LGK974<sup>18</sup> (Figure S1D). Reporter reflecting  $\beta$ -catenin-dependent transcription was also confirmed by the expression of *axin2*, a  $\beta$ -catenin target gene, at the AVC (Figure S1E).

Bone morphogenetic protein (Bmp) signaling activation and T-box transcription factor 2b (*tbx2b*) expression in AVC CMs reported in the paper<sup>19</sup> were confirmed using *Tg(BRE:EGFP)*<sup>20</sup> and *TgBAC(tbx2b:EGFP)*, respectively (Figures S1F–S1I). To know the spatial profiling of  $\beta$ -cat ON CMs and other CMs at the AVC, we detected  $\beta$ -cat ON CMs by red fluorescence using *Tg(myf7:GAL4db-TCF $\Delta$ C);Tg(5xUAS:NTR-mCherry)*, which is a  $\beta$ -cat ON reporter without 2A-mCherry (Figures 1D and 1E). *BRE:EGFP*<sup>+</sup> cells were mostly found in AVC CMs of the ventricle, while *tbx2b:EGFP*<sup>+</sup> cells were located in the root of AV valves (Figure S1J). Neither of them overlapped with  $\beta$ -cat ON CMs (Figures 1D, 1E, S1K, and S1L), suggesting that the AVC CMs can be grouped into three zones: Bmp signal<sup>+</sup>, Tbx2b<sup>+</sup>, and  $\beta$ -cat ON zones (Figure 1F).

### **$\beta$ -cat ON CMs at the AVC require heartbeat-dependent Wnt ligands**

We next tried to find Wnt ligands for  $\beta$ -cat ON CMs. Consistent with previous reports of myocardial *wnt2bb* and endocardial *wnt9b* expression at the AVC,<sup>21,22</sup> *wnt2bb* and *wnt9b* were expressed at the AVC at the embryonic stage (Figure 2A). To test the requirement of *wnt2bb* and *wnt9b* for  $\beta$ -cat ON CMs, we knocked down *wnt2bb* and *wnt9b* using morpholino oligonucleotides (MOs). The efficiency of MOs was confirmed by phenotypes of these gene mutants (Figures S2A–S2E).<sup>23</sup> Although the single knockdown was not sufficient, the *wnt2bb/wnt9b* double knockdown reduced the  $\beta$ -cat ON CM zone (Figures 2B and 2C). These data suggest that both Wnt2bb and Wnt9b contribute to Wnt/ $\beta$ -catenin signaling at the AVC. In juvenile fish, AVC CMs expressed *wnt2bb*, and AV valves expressed *wnt9b* (Figures S2F and S2G). Although *wnt9b* expression disappeared, *wnt2bb* was maintained in adults (Figures S2H and S2I). These data suggest a strong correlation between the specific expression of Wnt ligands and the specific  $\beta$ -cat ON CM zone at the AVC.

Next, we examined signals upstream of Wnt ligands. Not only *wnt9b* expression, which is reported to be regulated by mechanical force,<sup>22</sup> but also *wnt2bb* expression was decreased in the

troponin T type 2a (*tnnt2a*) morphants without heartbeat (Figure 2D). We therefore stopped the heartbeats of reporter embryos by *tnnt2a* MO or by 2,3-butanedione 2-monoxime (BDM), an inhibitor of muscle contraction. No  $\beta$ -cat ON CMs were observed in the heart without heartbeat (Figures 2E–2H). These data suggest that  $\beta$ -cat ON CMs require heartbeat-dependent Wnt ligand expression.

### **$\beta$ -cat ON CMs are required for coronary vascular formation**

To understand the function of  $\beta$ -cat ON CMs, we performed RNA-seq on  $\beta$ -cat ON and OFF CMs (Table S1). CMs were sorted from the AVC of *Tg(myf7:GAL4db-TCF $\Delta$ C-2A-mCherry);Tg(UAS:EGFP);Tg(myf7:NLS-mCherry)* fish (4~8 months old). Differentially expressed gene (DEG) analysis between  $\beta$ -cat ON and OFF CMs identified 1,491 DEGs. Wnt/ $\beta$ -catenin signaling target genes were upregulated in  $\beta$ -cat ON CMs (Figure 3A). Gene Ontology (GO) enrichment analysis identified that DEGs upregulated in  $\beta$ -cat ON CMs were related to vascular development (Figure 3B).

In zebrafish, coECs originate from endoECs at the AVC. CVs develop from 1 month of age and grow with age, body length, and ventricular size.<sup>8</sup> We hypothesized that  $\beta$ -cat ON CMs might induce the transition of endoECs to coECs. To observe CVs, we used *Tg(fli1:EGFP)* expressing EGFP under the EC- and blood cell-specific *fli1* (*Fli-1 proto-oncogene, ETS transcription factor*) promoter. *fli1:EGFP*<sup>+</sup> cells were observed at the AVC (9~10 mm in body length, at 1 month) and formed CVs (Figure 3C). Consistent with that the *fli1:EGFP*<sup>+</sup> cell at the AVC exhibited the angiogenic sprout in the *ex vivo* cultured heart (Figure S3A; Video S1C). When we observed ECs and  $\beta$ -cat ON CMs simultaneously, ECs penetrated  $\beta$ -cat ON CMs and connected with the surface CVs (Figures S3B and S3C), suggesting that ECs give rise to coECs during penetration of the  $\beta$ -cat ON CM zone.

To examine the involvement of  $\beta$ -cat ON CMs in CV formation, we depleted  $\beta$ -cat ON CMs by nitroreductase-metronidazole (NTR-MTZ) system.<sup>24</sup> An innocuous prodrug, MTZ, is enzymatically activated by NTR and induces apoptosis of NTR-expressing cells. To express NTR in the  $\beta$ -cat ON CMs, we developed *Tg(5xUAS:NTR-mCherry)* and confirmed the effectiveness of the NTR-MTZ system (Figure S3D). We further ablated NTR<sup>+</sup> cells in *Tg(fli1:EGFP)* background fish. MTZ was treated every 2 days for 42 days from the beginning of CV development (Figure 3D). CV outgrowth analyzed by the total length of *fli1:EGFP*<sup>+</sup> CVs was significantly inhibited in the  $\beta$ -cat ON CM-depleted fish (Figures 3E and 3F), indicating the requirement of  $\beta$ -cat ON CMs for CV growth.

To investigate the cause of CV growth defects in  $\beta$ -cat ON CM-ablated hearts, we examined CV length, CV coverage, and the number of EdU<sup>+</sup> proliferating coECs from  $\beta$ -cat ON CM-ablated hearts at an earlier time point (14-day treatment with MTZ). Although CV length and CV coverage were reduced in the  $\beta$ -cat ON CM-ablated hearts, EdU incorporation and the number of coEC were unchanged (Figures S3E–S3I), indicating reduced migration of ECs in the  $\beta$ -cat ON CM-ablated hearts. When  $\beta$ -cat ON CMs were ablated in mature fish (at 3 months), CV length was not affected (Figures S3J and S3K). These data suggest that  $\beta$ -cat ON CMs contribute to CV migration but not to EC proliferation and CV maintenance.

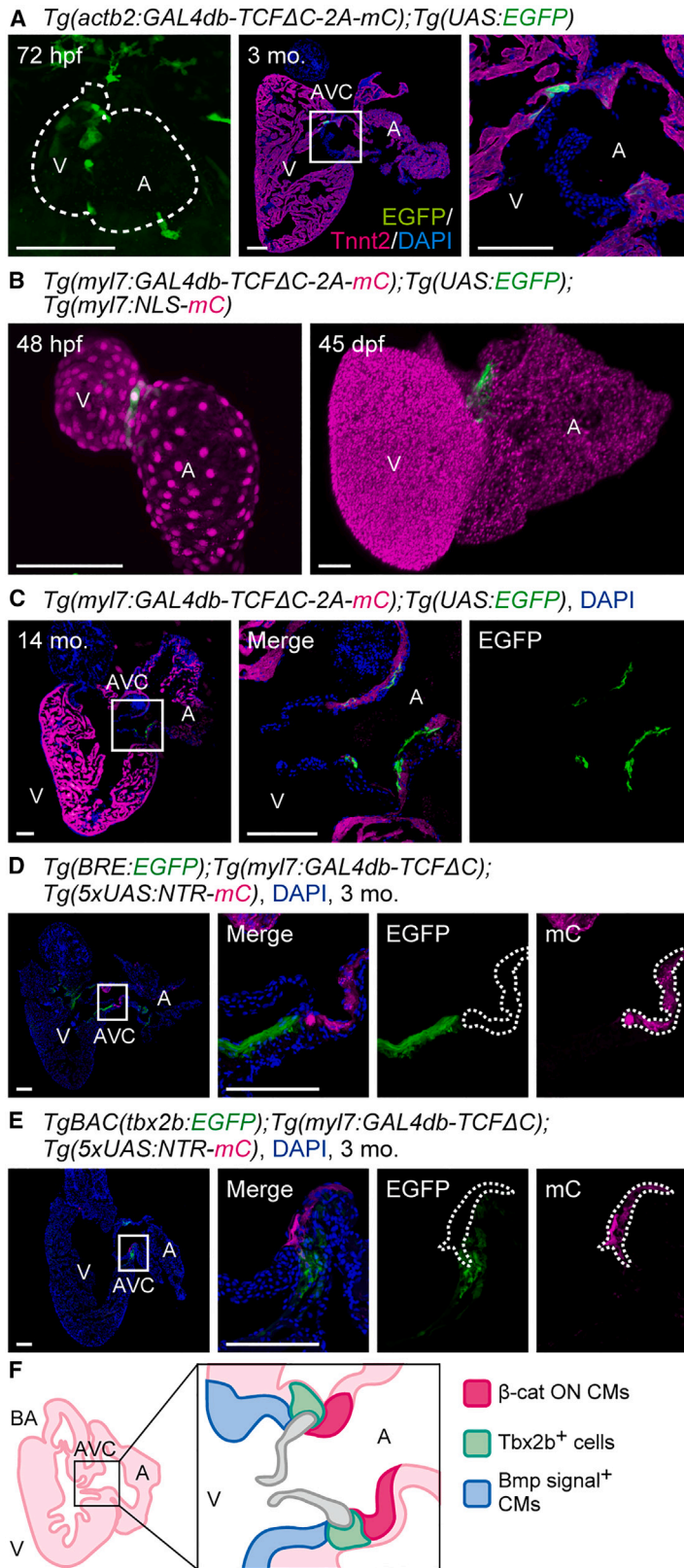


**Figure 1. Myocardial Wnt/ $\beta$ -catenin signal-activated zone exists at the AVC in embryonic and adult stages**

(A) Representative confocal images of the hearts of *Tg(actb2:GAL4db-TCF $\Delta$ C-2A-mCherry);Tg(UAS:EGFP)* fish. A ventral view of the heart at 72 h post-fertilization (hpf) (left). A cryosection image of the heart at 3 months stained with anti-GFP and anti-troponin T type 2 (Tnnt2) antibodies and 4',6-diamidino-2-phenylindole (DAPI) (center). The boxed region is enlarged (right). Dotted lines outline the heart. Images shown in all figures are 3D-rendered confocal images of a stack unless otherwise noted. Confocal images in all figures are representative of at least three individuals.

(B) Representative images of the hearts of *Tg(myI7:GAL4db-TCF $\Delta$ C-2A-mCherry);Tg(UAS:EGFP);Tg(myI7:NLS-mCherry)* fish. A ventral view of the heart at 48 hpf (left). A resected heart at 45 days post-fertilization (dpf) was made transparent with clear, unobstructed brain/body imaging cocktails and computational analysis reagent-1A (CUBIC-1A) (right). *Tg(myI7:NLS-mCherry)* was used to outline the heart shape because the fluorescence of *myI7:NLS-mCherry* is brighter than that of *myI7:GAL4db-TCF $\Delta$ C-2A-mCherry*.

(C) A representative cryosection image of the heart of a 14-month-old *Tg(myI7:GAL4db-TCF $\Delta$ C-2A-mCherry);Tg(UAS:EGFP)* fish stained with DAPI (left). The boxed region is enlarged (center and right). The fluorescence channel is indicated at the top.

(D) A representative cryosection image of the heart of a 3-month-old *Tg(BRE:EGFP);Tg(myI7:GAL4db-TCF $\Delta$ C);Tg(5xUAS:NTR-mCherry)* fish stained with DAPI (left). The boxed region is enlarged (right). Bmp signal<sup>+</sup> cells do not overlap with  $\beta$ -cat ON CMs (dotted lines).

(E) A representative cryosection image of the heart of a *TgBAC(tbx2b:EGFP);Tg(myI7:GAL4db-TCF $\Delta$ C);Tg(5xUAS:NTR-mCherry)* fish at 3 months stained with DAPI (left). The boxed region is enlarged (right). Tbx2b<sup>+</sup> cells do not overlap with  $\beta$ -cat ON CMs (dotted lines).

(F) Schematic zonation at the AVC demarcated by the markers.  $\beta$ -cat ON CMs, Tbx2b<sup>+</sup> cells, and Bmp signal<sup>+</sup> cells were observed in the CMs at the atrial side of the AVC, at the root of the valves, and on the ventricular side of the AVC, respectively.

Scale bars, 100  $\mu$ m. A, atrium; AVC, atrioventricular canal; BA, bulbus arteriosus; CM, cardiomyocyte; mo, month; V, ventricle.

See also [Figure S1](#) and [Videos S1A](#) and [S1B](#).

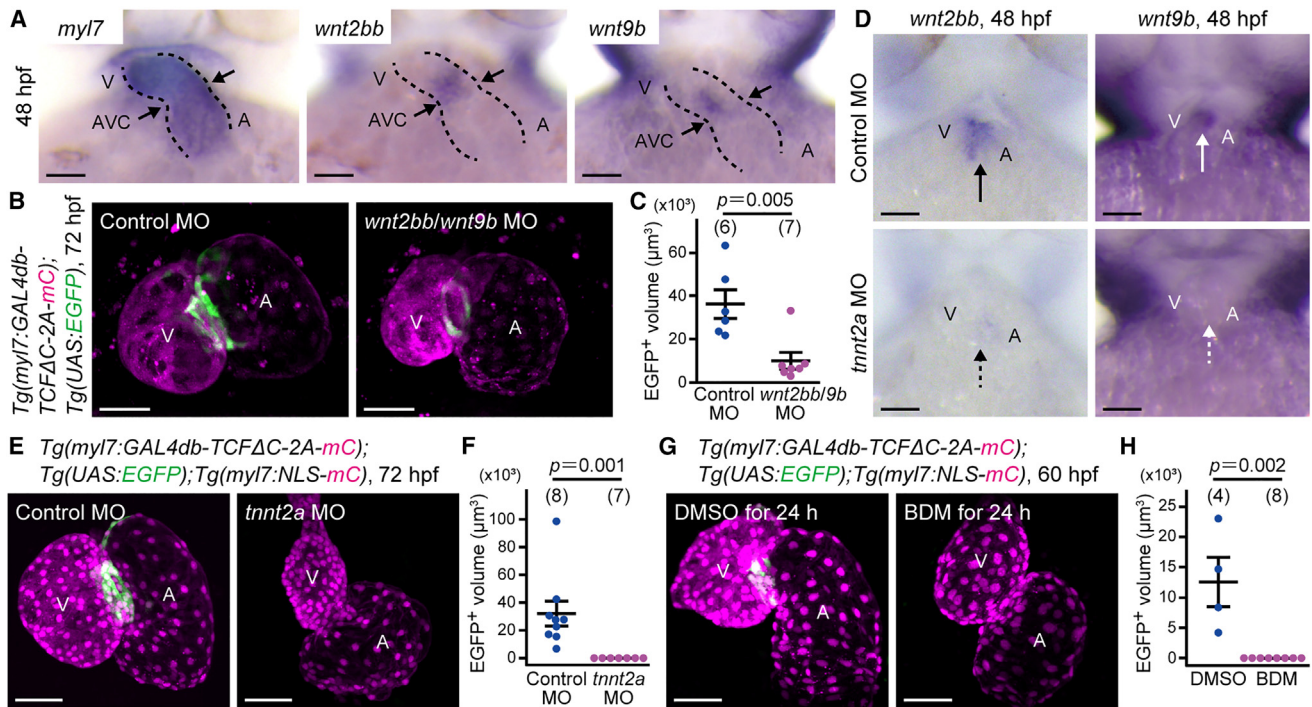


**Figure 2. Heartbeat-dependent Wnt expression turns on Wnt/ $\beta$ -catenin signaling in AVC CMs**

(A) Representative stereomicrographs of whole-mount *in situ* hybridization (WISH) analyses of *myl7* (left), *wnt2bb* (center), and *wnt9b* (right) mRNA expression in three zebrafish embryos at 48 hpf. Ventral views. Dotted lines outline the heart. Arrows indicate the AVC.

(B) Representative images of the hearts of *Tg(myl7:GAL4db-TCF $\Delta$ C-2A-mCherry);Tg(UAS:EGFP)* larvae at 72 hpf injected with 7 ng control morpholino oligonucleotide (MO) (left) and 5 ng *wnt2bb* and 2 ng *wnt9b* MO (right).

(C) Quantitative analysis of the data shown in (B). The volume of the UAS:EGFP<sup>+</sup> region was measured. In this and the following graphs, unless otherwise described, each dot represents an individual fish, and the number of fish analyzed is indicated at the top.

(D) Representative stereomicrographs of WISH analyses of *wnt2bb* (left) and *wnt9b* (right) mRNA expression in four embryos at 48 hpf. Embryos were injected with 2 ng control MO (top) and 2 ng *tnt2a* MO (bottom). Arrows and broken arrows indicate positive and less mRNA expression, respectively.

(E) Representative images of the hearts of *Tg(myl7:GAL4db-TCF $\Delta$ C-2A-mCherry);Tg(UAS:EGFP);Tg(myl7:NLS-mCherry)* larvae at 72 hpf injected with 2 ng control MO (left) and 2 ng *tnt2a* MO (right).

(F) Quantitative analysis of the data shown in (E).

(G) Representative images of the hearts of *Tg(myl7:GAL4db-TCF $\Delta$ C-2A-mCherry);Tg(UAS:EGFP);Tg(myl7:NLS-mCherry)* embryos at 60 hpf treated with DMSO (left) or 20 mM 2,3-butanedione 2-monoxime (BDM) (right) for 24 h.

(H) Quantitative analysis of the data shown in (G).

Scale bars, 50  $\mu$ m. Data are mean  $\pm$  SEM. Statistical analysis was performed by Mann-Whitney U test.

See also [Figure S2](#).

We also examined the contribution of Tbx2b<sup>+</sup> cells in another zone of AVC to CV development by ablating Tbx2b<sup>+</sup> cells. Although Tbx2b<sup>+</sup> cells were successfully depleted, CV development was not affected ([Figures S3L–S3N](#)). Therefore, the  $\beta$ -cat ON CM zone might be a specific zone involved in the regulation of CV development.

To confirm the requirement of Wnt/ $\beta$ -catenin signaling for CV development, we examined the effect of IWR1 on the growth of coECs. The IWR1 treatment remarkably reduced the CV length ([Figures S3O and S3P](#)). Because Wnt/ $\beta$ -catenin signaling in coECs ([Figure S3Q](#)) promotes coEC proliferation,<sup>25</sup> we inhibited Wnt/ $\beta$ -catenin signaling in CMs using a dominant negative form of TCF (TCF $\Delta$ N).<sup>14</sup> To avoid embryonic lethality,<sup>6</sup> we established inducible expression of TCF $\Delta$ N by developing two Tg lines: *Tg(myl7:GvEcR)* and *Tg(5xUAS:TCF $\Delta$ N-mCherry)*. The former Tg expresses an ecdysone receptor-dependent (EcR-dependent) expression of GAL4 in CMs. The latter expresses

TCF $\Delta$ N under UAS. We induced TCF $\Delta$ N expression during CV development by treatment with tebufenozide, an EcR agonist ([Figure 3G](#)). CV length was reduced by TCF $\Delta$ N expression ([Figures 3H and 3I](#)). The inhibitory effect of TCF $\Delta$ N was confirmed by the impaired heart looping and the reduction of *axin2* ([Figures S3R and S3S](#)). These data suggest that Wnt/ $\beta$ -catenin signaling activated in the CMs is required for CV development.

### $\beta$ -cat ON CMs induce arterialization of immature CVs

We next tried to understand how  $\beta$ -cat ON CMs promote CV formation. To compare the gene expression between CVs of the hearts with and without  $\beta$ -cat ON CMs, we performed scRNA-seq of sorted *flil1:EGFP*<sup>+</sup> cells from control and  $\beta$ -cat ON CM-ablated hearts ([Figure 4A](#)). The 4,214 cells and 5,230 cells from hearts with and without  $\beta$ -cat ON CMs, respectively, were plotted in uniform manifold approximation and projection

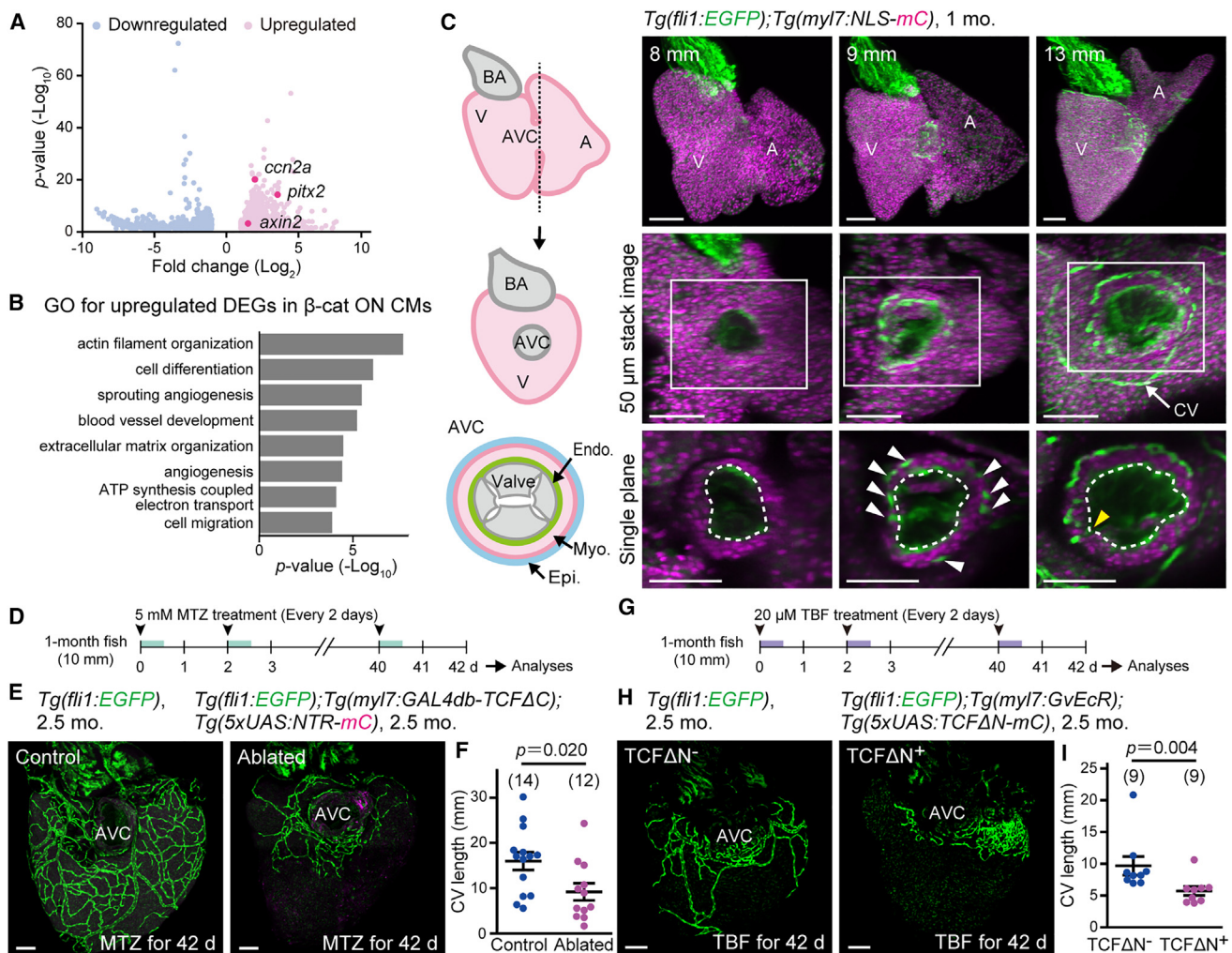


**Figure 3.  $\beta$ -cat ON CMs contribute to CV formation**

(A) A volcano plot showing differentially expressed genes (DEGs) between  $\beta$ -cat ON and OFF CMs ( $n = 3$ ). Note that Wnt target genes (red circle) were upregulated.

(B) Gene Ontology (GO) enrichment analysis of genes upregulated in  $\beta$ -cat ON CMs.

(C) Schematic illustration of the heart (left) and representative images of the hearts of 1-month-old *Tg(fli1:EGFP);Tg(myf7:NLS-mCherry)* fish with body length indicated at the top (right). Hearts were made transparent with CUBIC-1A. Lateral projections (top), 50  $\mu\text{m}$  stacked images of the dorsal view around the AVC (middle), and single slice images of the boxed regions (bottom). Dotted lines outline the heart lumen. Endothelial cells (ECs) are observed in the CM layer (white arrowheads). Coronary vessels (CVs) connect with endoECs at the AVC (yellow arrowhead).

(D) Experimental design for specific ablation of nitroreductase-expressing (NTR-expressing) cells of the fish used in (E) by metronidazole (MTZ) treatment. 1-month-old fish were treated with 5 mM MTZ every 2 days and analyzed after 42 days of treatment.

(E) Representative images of the CVs of *Tg(fli1:EGFP)* or *Tg(fli1:EGFP);Tg(myf7:GAL4db-TCF $\Delta$ C);Tg(5xUAS:NTR-mCherry)* fish at 2.5 months treated with MTZ. A control heart (left) and a  $\beta$ -cat ON CM-ablated heart (right).

(F) Quantitative analysis of the data shown in (E). The length of CVs was measured by tracing the length of *fli1:EGFP*<sup>+</sup> coECs.

(G) Experimental design for CM-specific induction of dominant negative TCF (TCF $\Delta$ N) by tebufenozide (TBF) treatment in the fish used in (H). Fish were treated with 20  $\mu\text{M}$  TBF every 2 days and analyzed after 42 days.

(H) Representative images of the CVs of *Tg(fli1:EGFP)* or *Tg(fli1:EGFP);Tg(myf7:GvEcR);Tg(5xUAS:TCF $\Delta$ N-mCherry)* fish at 2.5 months treated with TBF. A control heart (left) or a TCF $\Delta$ N-expressed heart (right).

(I) Quantitative analysis of the data shown in (H).

Scale bars, 100  $\mu\text{m}$ . Data are mean  $\pm$  SEM. Statistical analysis was performed by two-tailed Student's  $t$  test (F) or Mann-Whitney U test (I). CV, coronary vessel; Endo, endocardium; Epi, epicardium; Myo, myocardium.

See also [Figure S3](#), [Table S1](#), and [Video S1C](#).

(UMAP) space ([Figures 4B](#) and [S4A](#); [Table S2](#)). According to the expression of marker genes,<sup>26,27</sup> we classified the cells into 9 cell types ([Figure 4B](#)). About 94% of the cells were ECs ([Figure S4B](#)).

The coEC cluster expressed the known marker genes<sup>27,28</sup> ([Figure 4C](#)). The expression of several marker genes on coEC was confirmed ([Figures S4C](#) and [S4D](#)). GO enrichment analysis

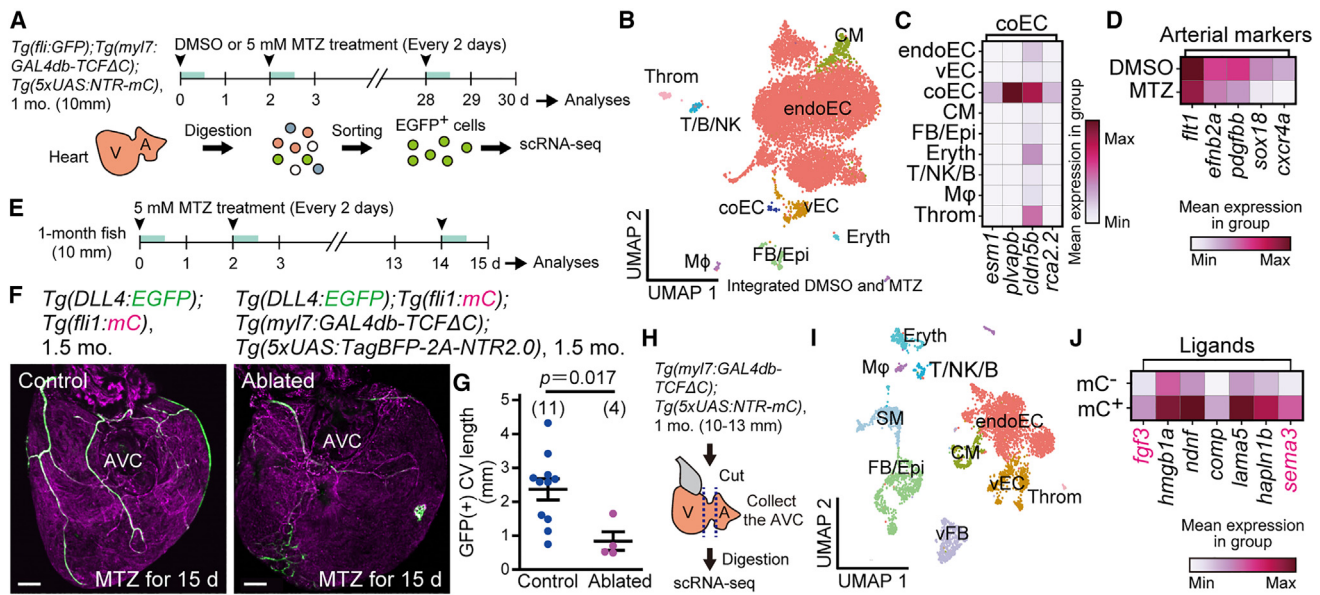


**Figure 4.  $\beta$ -cat ON CMs are required for CV arterialization**

(A) An experimental design of preparation of cells followed by scRNA-seq. *fli1:EGFP*<sup>+</sup> cells were collected from the fish treated with DMSO or 5 mM MTZ every 2 days.

(B) Uniform manifold approximation and projection (UMAP) visualization of integrated cells from DMSO-treated and MTZ-treated hearts. Cells are color-coded by type. endoEC, endocardial EC; coEC, coronary EC; vEC, valvular EC; Epi, epicardial cells; FB, fibroblasts; Eryth, erythrocytes; T, T cells; NK, natural killer cells; B, B cells; M $\phi$ , macrophages; Throm, thrombocytes.

(C) A matrix plot of coEC marker gene expression (bottom) in each cluster (left) shown in (B).

(D) A matrix plot of arterial marker gene expression (bottom) of coECs from hearts treated with DMSO (upper) or MTZ (lower).

(E) Experimental design to analyze the CV of the fish used in (F). Fish were treated with 5 mM MTZ every 2 days and analyzed after 15 days of treatment.

(F) Representative images of arteries and CVs of control or *Tg(DLL4:EGFP);Tg(myf17:GAL4db-TCF $\Delta$ C);Tg(5xUAS:TagBFP-2A-NTR2.0)* fish at 1.5 months treated with MTZ. A control heart (left) and a  $\beta$ -cat ON CM-ablated heart (right).

(G) Quantitative analysis of the data shown in (F).

(H) Experimental design for preparing the cells at the AVC followed by scRNA-seq. The fish indicated at the top treated with DMSO for 48 h were used.

(I) UMAP visualization of cells obtained from the AVC of the fish in (H) at 1 month. Cells are color-coded by type. vFB, valvular FB; SM, smooth muscle cells.

(J) A matrix plot of ligand expression (bottom) in  $\beta$ -cat OFF ( $mC^-$ ) and ON ( $mC^+$ ) CMs of the AVCs at 1 month.

Scale bars, 100  $\mu$ m. Data are mean  $\pm$  SEM. Statistical analysis was performed by two-tailed Student's t test. BF, bright field. See also [Figure S4](#) and [Table S2](#).

identified that DEGs upregulated in DMSO-treated coECs compared with MTZ-treated coECs were associated with artery development ([Figure S4E](#)). Several arterial markers<sup>29,30</sup> were reduced in the MTZ-treated coECs ([Figure 4D](#)). Since arterialization is an important step during CV maturation<sup>8</sup> and corresponds to migratory signaling,<sup>31</sup> we confirmed the reduction of arterialization by qPCR of the *ephrin-B2a* (*efnb2a*) gene ([Figure S4F](#)). Furthermore, we confirmed the inhibition of arterialization by the ablation of  $\beta$ -cat ON CM in the *Tg(Dll4:EGFP)* fish in which arteries are marked by EGFP. The depletion of  $\beta$ -cat ON CMs by NTR2.0<sup>32</sup> fused with BFP resulted in a decreased number of thick arteries and a decrease in the total length of *DLL4:EGFP*<sup>+</sup> arteries, suggesting the requirement of  $\beta$ -cat ON CMs for arterialization of CVs ([Figures 4E–4G](#) and [S4G](#)).

To understand how  $\beta$ -cat ON CMs regulate CVs, we tried to search for EC-trophic ligands expressed in the  $\beta$ -cat ON CMs by performing scRNA-seq of the cells collecting from the AVC of  $\beta$ -cat ON reporter fish that started growth of CVs (10–13 mm in body length, at 1 month) ([Figure 4H](#); [Table S2](#)). The cells were classified into 10 cell types and plotted on UMAP ([Figure 4I](#)). We identified the 7 genes encoding extracel-

lular ligands whose expression was higher in  $\beta$ -cat ON CMs ( $mC^+$ ) than in OFF CMs ( $mC^-$ ) ([Figure 4J](#)). To examine the dependency of Wnt/ $\beta$ -catenin signaling, we also performed scRNA-seq with an IWR1-treated sample ([Figures S4H–S4J](#); [Table S2](#)). The expression of the ligands upregulated in  $\beta$ -cat ON CMs was reduced by IWR1 treatment ([Figure S4K](#)). Among these potential EC-trophic ligands, fibroblast growth factor 3 (*fgf3*) and *si:dkey-49n23.1*, a gene coding semaphorin 3D (Sema3d), are reported to be involved in vascular formation.<sup>33–35</sup> Consistently, receptors for Fgfs and Semas were detected in the EC cluster ([Figure S4L](#)), suggesting that these ligands might be potential candidates to regulate CV formation.

## DISCUSSION

Inter- and intra-organ heterogeneity among various types of cells has been identified by scRNA-seq. However, the spatial and functional heterogeneity of CMs has not been well investigated. We focused on  $\beta$ -cat ON cells as a marker of zonation by comparing other signals and identifying the zones at the AVC. Although we demonstrated heartbeat-dependent Wnts as

regulators of  $\beta$ -cat ON CMs, other factors may also regulate zonation. In our RNA-seq data, the upregulation of *frizzleds* was restricted in  $\beta$ -cat ON cells (Table S1). Thus, spatial and temporal expression of ligands and receptors determines the special signal-responsive zone in the heart. The combination of scRNA-seq and signal reporter models helps us to find functional zones *in vivo*.

The  $\beta$ -cat ON CM zone is a specific zone promoting CV migration and coEC maturation through arterialization. The incomplete arterialization resulted in defects of coEC migration. Therefore, we tried to understand how  $\beta$ -cat ON CMs promote the arterialization of ECs. We searched for potential EC-trophic ligands secreted from  $\beta$ -cat ON CMs and identified *Sema3d* and *Fgf3* by scRNA-seq. *Sema3d* regulates CV migration.<sup>34</sup> Fgfs induce vascularization<sup>33</sup> and vessel maturation by enhancing the vascular endothelial growth factor (*Vegf*) pathway.<sup>35</sup> Although BMP2 and VEGF are key molecules for the transition from endoEC to CV in mice,<sup>36</sup> neither *bmp2* nor *vegfa* was upregulated in  $\beta$ -cat ON CMs (Tables S1 and S2). Details of *Sema3a*- and *Fgf3*-dependent signals will need to be investigated.

CVs develop continuously in adult zebrafish.<sup>37</sup> However,  $\beta$ -cat ON CMs did not contribute to CV development in mature hearts (Figures S3J and S3K).  $\beta$ -cat ON CMs that exist at the AVC even after the establishment of the CV network might have other roles, such as maintenance of the AV valves.

Identifying the mechanism of developmental CV formation and maintenance or regrowth of CV is important because re-activation of CV growth could help CV regeneration in injured hearts. Further investigation of secretory factors expressed in  $\beta$ -cat ON CMs will help us to find the therapeutic target for the regeneration of the injured heart.

### Limitations of the study

In this study, we could not show whether *Fgf3* and *Sema3d* secreted by  $\beta$ -cat ON CMs regulate CV formation. The mechanism regulating the development of endoEC into CVs by  $\beta$ -cat ON CMs remains unclear and should be addressed in future studies.

### RESOURCE AVAILABILITY

#### Lead contact

Further information and requests for resources and reagents should be directed to and will be fulfilled by the lead contact, Naoki Mochizuki ([mochizuki@ncvc.go.jp](mailto:mochizuki@ncvc.go.jp)).

#### Materials availability

Further information and requests for resources and reagents listed in the [key resources table](#) should be directed to the [lead contact](#).

#### Data and code availability

RNA-seq and scRNA-seq data were deposited in the Gene Expression Omnibus under accession number GEO: GSE223462. This paper does not report the original code. Any additional information required to reanalyze the data reported in this paper is available from the [lead contact](#) upon request.

### ACKNOWLEDGMENTS

We thank K. Kawakami (National Institute of Genetics, Japan) for the Tol2 system and *Tg(UAS:EGFP)* fish; D.Y. Stainier (Max Planck Institute, Germany) for pcDNA-NTR; S. Fukuhara and S. Yuge (Nippon Med. School, Japan) for *Tg(DLL4:EGFP)*; K. Terai and Y. Sando (Next-generation sequencing core fa-

cility of the Graduate Schools of Biostudies, Kyoto University, Japan) for support of the RNA-seq analysis; J.T. Pearson for critical reading; M. Sone, K. Hiratomi, T. Sato, T. Mabuchi, and T. Babazono for excellent technical assistance; and S. Toyoshima for fish care. This work was supported in part by grants from JSPS KAKENHI (no. 18K15025 and 22K15156 to A.C. and 19H01022 to N.M.), JST (JPMJPF2018 and JPMJMS2024-3 to N.M.), and Takeda Science Foundation (to N.M.). This work was supported by COI-NEXT Support Unit for Imaging Science at Kento.

### AUTHOR CONTRIBUTIONS

Conceptualization, A.C. and N.M.; formal analysis, A.C., M.S., and T.Y.; investigation, A.C. and M.F.; resources, A.C., H.F., and H.N.; writing – original draft, A.C. and N.M.; writing – review and editing, A.C., H.N., T.Y., and N.M.; visualization, A.C.; supervision, N.M.; project administration, N.M.; funding acquisition, A.C. and N.M.

### DECLARATION OF INTERESTS

The authors declare no competing interests.

### STAR★METHODS

Detailed methods are provided in the online version of this paper and include the following:

- KEY RESOURCES TABLE
- EXPERIMENTAL MODEL AND SUBJECT DETAILS
  - Animal studies
- METHOD DETAILS
  - Plasmids
  - BAC recombineering
  - Transgenic zebrafish lines
  - Genotyping
  - Microinjection of oligonucleotide
  - Chemical treatment
  - Imaging
  - Sectioning of zebrafish hearts
  - Immunohistochemistry (IHC)
  - EdU staining
  - *in situ* hybridization (ISH)
  - RNAscope assay
  - Alcian blue staining
  - Tissue clearing
  - Cell sorting
  - RNA sequencing (RNA-seq)
  - single-cell RNA sequencing (scRNA-seq)
  - Quantitative PCR (qPCR)
- QUANTIFICATION AND STATISTICAL ANALYSIS
  - $\beta$ -cat ON CM volume measurement
  - CV length measurement
  - Coverage measurement
  - coEC and EdU<sup>+</sup> coEC measurement
  - Head length measurement
  - Statistical analysis

### SUPPLEMENTAL INFORMATION

Supplemental information can be found online at <https://doi.org/10.1016/j.devcel.2024.09.012>.

Received: March 17, 2023

Revised: April 18, 2024

Accepted: September 11, 2024

Published: October 11, 2024

## REFERENCES

- Kohl, P. (2004). Cardiac cellular heterogeneity and remodelling. *Cardiovasc. Res.* 64, 195–197. <https://doi.org/10.1016/j.cardiores.2004.08.011>.
- Chen, L., Hua, K., Zhang, N., Wang, J., Meng, J., Hu, Z., Gao, H., Li, F., Chen, Y., Ren, J., et al. (2022). Multifaceted spatial and functional zonation of cardiac cells in adult human heart. *Circulation* 145, 315–318. <https://doi.org/10.1161/CIRCULATIONAHA.121.055690>.
- Litviňuková, M., Talavera-López, C., Maatz, H., Reichart, D., Worth, C.L., Lindberg, E.L., Kanda, M., Polanski, K., Heinig, M., Lee, M., et al. (2020). Cells of the adult human heart. *Nature* 588, 466–472. <https://doi.org/10.1038/s41586-020-2797-4>.
- Vanlandewijck, M., He, L., Mäe, M.A., Andrae, J., Ando, K., Del Gaudio, F., Nahar, K., Lebouvier, T., Laviña, B., Gouveia, L., et al. (2018). A molecular atlas of cell types and zonation in the brain vasculature. *Nature* 554, 475–480. <https://doi.org/10.1038/nature25739>.
- Nusse, R., and Clevers, H. (2017). Wnt/ $\beta$ -catenin signaling, disease, and emerging therapeutic modalities. *Cell* 169, 985–999. <https://doi.org/10.1016/j.cell.2017.05.016>.
- Hurlstone, A.F.L., Haramis, A.-P.G., Wienholds, E., Begthel, H., Korving, J., van Eeden, F., Cuppen, E., Zivkovic, D., Plasterk, R.H.A., and Clevers, H. (2003). The Wnt/ $\beta$ -catenin pathway regulates cardiac valve formation. *Nature* 425, 633–637. <https://doi.org/10.1038/nature02028>.
- Gillers, B.S., Chiuplunkar, A., Aly, H., Valenta, T., Basler, K., Christoffels, V.M., Efimov, I.R., Boukens, B.J., and Rentschler, S. (2015). Canonical Wnt signaling regulates atrioventricular junction programming and electrophysiological properties. *Circ. Res.* 116, 398–406. <https://doi.org/10.1161/CIRCRESAHA.116.304731>.
- Harrison, M.R.M., Bussmann, J., Huang, Y., Zhao, L., Osorio, A., Burns, C.G., Burns, C.E., Sucov, H.M., Siekmann, A.F., and Lien, C.L. (2015). Chemokine-guided angiogenesis directs coronary vasculature formation in zebrafish. *Dev. Cell* 33, 442–454. <https://doi.org/10.1016/j.devcel.2015.04.001>.
- Red-Horse, K., Ueno, H., Weissman, I.L., and Krasnow, M.A. (2010). Coronary arteries form by developmental reprogramming of venous cells. *Nature* 464, 549–553. <https://doi.org/10.1038/nature08873>.
- Wu, B., Zhang, Z., Lui, W., Chen, X., Wang, Y., Chamberlain, A.A., Moreno-Rodriguez, R.A., Markwald, R.R., O'Rourke, B.P., Sharp, D.J., et al. (2012). Endocardial cells form the coronary arteries by angiogenesis through myocardial-endocardial VEGF signaling. *Cell* 151, 1083–1096. <https://doi.org/10.1016/j.cell.2012.10.023>.
- Benhamouche, S., Decaens, T., Godard, C., Chambrey, R., Rickman, D.S., Moïnard, C., Vasseur-Cognet, M., Kuo, C.J., Kahn, A., Perret, C., et al. (2006). Apc tumor suppressor gene is the “zonation-keeper” of mouse liver. *Dev. Cell* 10, 759–770. <https://doi.org/10.1016/j.devcel.2006.03.015>.
- Berthon, A., Drelon, C., Ragazzon, B., Boulkroun, S., Tissier, F., Amar, L., Samson-Couterie, B., Zennaro, M.C., Plouin, P.F., Skah, S., et al. (2014). WNT/ $\beta$ -catenin signalling is activated in aldosterone-producing adenomas and controls aldosterone production. *Hum. Mol. Genet.* 23, 889–905. <https://doi.org/10.1093/hmg/ddt484>.
- Paris, J., and Henderson, N.C. (2022). Liver zonation, revisited. *Hepatology* 76, 1219–1230. <https://doi.org/10.1002/hep.32408>.
- Kashiwada, T., Fukuhara, S., Terai, K., Tanaka, T., Wakayama, Y., Ando, K., Nakajima, H., Fukui, H., Yuge, S., Saito, Y., et al. (2015).  $\beta$ -catenin-dependent transcription is central to bmp-mediated formation of venous vessels. *Development* 142, 497–509. <https://doi.org/10.1242/dev.115576>.
- Moro, E., Ozhan-Kizil, G., Mongera, A., Beis, D., Wierzbicki, C., Young, R.M., Bournele, D., Domenichini, A., Valdivia, L.E., Lum, L., et al. (2012). In vivo Wnt signaling tracing through a transgenic biosensor fish reveals novel activity domains. *Dev. Biol.* 366, 327–340. <https://doi.org/10.1016/j.ydbio.2012.03.023>.
- Pestel, J., Ramadass, R., Gauvrit, S., Helker, C., Herzog, W., and Stainier, D.Y.R. (2016). Real-time 3D visualization of cellular rearrangements during cardiac valve formation. *Development* 143, 2217–2227. <https://doi.org/10.1242/dev.133272>.
- Chen, B., Dodge, M.E., Tang, W., Lu, J., Ma, Z., Fan, C.W., Wei, S., Hao, W., Kilgore, J., Williams, N.S., et al. (2009). Small molecule-mediated disruption of Wnt-dependent signaling in tissue regeneration and cancer. *Nat. Chem. Biol.* 5, 100–107. <https://doi.org/10.1038/nchembio.137>.
- Liu, J., Pan, S., Hsieh, M.H., Ng, N., Sun, F., Wang, T., Kasibhatla, S., Schuller, A.G., Li, A.G., Cheng, D., et al. (2013). Targeting Wnt-driven cancer through the inhibition of Porcupine by LGK974. *Proc. Natl. Acad. Sci. USA* 110, 20224–20229. <https://doi.org/10.1073/pnas.1314239110>.
- Singh, R., Horsthuis, T., Farin, H.F., Grieskamp, T., Norden, J., Petry, M., Wakker, V., Moorman, A.F.M., Christoffels, V.M., and Kispert, A. (2009). Tbx20 interacts with smads to confine tbx2 expression to the atrioventricular canal. *Circ. Res.* 105, 442–452. <https://doi.org/10.1161/CIRCRESAHA.109.196063>.
- Collery, R.F., and Link, B.A. (2011). Dynamic smad-mediated BMP signaling revealed through transgenic zebrafish. *Dev. Dyn.* 240, 712–722. <https://doi.org/10.1002/dvdy.22567>.
- Nguyen, C.T., Langenbacher, A., Hsieh, M., and Chen, J.N. (2010). The PAF1 complex component Leo1 is essential for cardiac and neural crest development in zebrafish. *Dev. Biol.* 341, 167–175. <https://doi.org/10.1016/j.ydbio.2010.02.020>.
- Goddard, L.M., Duchemin, A.L., Ramalingan, H., Wu, B., Chen, M., Bamezai, S., Yang, J., Li, L., Morley, M.P., Wang, T., et al. (2017). Hemodynamic forces sculpt developing heart valves through a KLF2-WNT9B paracrine signaling axis. *Dev. Cell* 43, 274–289.e5. <https://doi.org/10.1016/j.devcel.2017.09.023>.
- Ober, E.A., Verkade, H., Field, H.A., and Stainier, D.Y.R. (2006). Mesodermal Wnt2b signalling positively regulates liver specification. *Nature* 442, 688–691. <https://doi.org/10.1038/nature04888>.
- Curado, S., Anderson, R.M., Jungblut, B., Mumm, J., Schroeter, E., and Stainier, D.Y.R. (2007). Conditional targeted cell ablation in zebrafish: a new tool for regeneration studies. *Dev. Dyn.* 236, 1025–1035. <https://doi.org/10.1002/dvdy.21100>.
- Da Silva, F., Rocha, A.S., Motamedi, F.J., Massa, F., Basboga, C., Morrison, H., Wagner, K.D., and Schedl, A. (2017). Coronary artery formation is driven by localized expression of R-spondin3. *Cell Rep.* 20, 1745–1754. <https://doi.org/10.1016/j.celrep.2017.08.004>.
- Ma, H., Liu, Z., Yang, Y., Feng, D., Dong, Y., Garbutt, T.A., Hu, Z., Wang, L., Luan, C., Cooper, C.D., et al. (2021). Functional coordination of non-myocytes plays a key role in adult zebrafish heart regeneration. *EMBO Rep.* 22, e52901. <https://doi.org/10.15252/embr.202152901>.
- Hu, B., Lelek, S., Spanjaard, B., El-Sammak, H., Simões, M.G., Mintcheva, J., Aliee, H., Schäfer, R., Meyer, A.M., Theis, F., et al. (2022). Origin and function of activated fibroblast states during zebrafish heart regeneration. *Nat. Genet.* 54, 1227–1237. <https://doi.org/10.1038/s41588-022-01129-5>.
- Li, Z., Solomonidis, E.G., Meloni, M., Taylor, R.S., Duffin, R., Dobbie, R., Magalhaes, M.S., Henderson, B.E.P., Louwe, P.A., D'Amico, G., et al. (2019). Single-cell transcriptome analyses reveal novel targets modulating cardiac neovascularization by resident endothelial cells following myocardial infarction. *Eur. Heart J.* 40, 2507–2520. <https://doi.org/10.1093/eurheartj/ehz305>.
- Stratman, A.N., Burns, M.C., Farrelly, O.M., Davis, A.E., Li, W., Pham, V.N., Castranova, D., Yano, J.J., Goddard, L.M., Nguyen, O., et al. (2020). Chemokine mediated signalling within arteries promotes vascular smooth muscle cell recruitment. *Commun. Biol.* 3, 734. <https://doi.org/10.1038/s42003-020-01462-7>.
- Lawson, N.D., Scheer, N., Pham, V.N., Kim, C.H., Chitnis, A.B., Campos-Ortega, J.A., and Weinstein, B.M. (2001). Notch signaling is required for arterial-venous differentiation during embryonic vascular development. *Development* 128, 3675–3683. <https://doi.org/10.1242/dev.128.19.3675>.
- Luo, W., Garcia-Gonzalez, I., Fernández-Chacón, M., Casquero-García, V., Sanchez-Muñoz, M.S., Mühleder, S., Garcia-Ortega, L., Andrade, J., Potente, M., and Bedito, R. (2021). Arterialization requires the timely

- suppression of cell growth. *Nature* 589, 437–441. <https://doi.org/10.1038/s41586-020-3018-x>.
32. Sharrock, A.V., Mulligan, T.S., Hall, K.R., Williams, E.M., White, D.T., Zhang, L., Emmerich, K., Matthews, F., Nimmagadda, S., Washington, S., et al. (2022). NTR 2.0: a rationally engineered prodrug-converting enzyme with substantially enhanced efficacy for targeted cell ablation. *Nat. Methods* 19, 205–215. <https://doi.org/10.1038/s41592-021-01364-4>.
  33. Liu, F., Pogoda, H.M., Pearson, C.A., Ohyama, K., Löhner, H., Hammerschmidt, M., and Placzek, M. (2013). Direct and indirect roles of Fgf3 and Fgf10 in innervation and vascularisation of the vertebrate hypothalamic neurohypophys. *Development* 140, 1111–1122. <https://doi.org/10.1242/dev.080226>.
  34. Aghajanian, H., Cho, Y.K., Manderfield, L.J., Herling, M.R., Gupta, M., Ho, V.C., Li, L., Degenhardt, K., Aharonov, A., Tzahor, E., et al. (2016). Coronary vasculature patterning requires a novel endothelial ErbB2 holoreceptor. *Nat. Commun.* 7, 12038. <https://doi.org/10.1038/ncomms12038>.
  35. Murakami, M., and Simons, M. (2008). Fibroblast growth factor regulation of neovascularization. *Curr. Opin. Hematol.* 15, 215–220. <https://doi.org/10.1097/MOH.0b013e3282f97d98>.
  36. D'Amato, G., Phansalkar, R., Naftaly, J.A., Fan, X., Amir, Z.A., Rios Coronado, P.E., Cowley, D.O., Quinn, K.E., Sharma, B., Caron, K.M., et al. (2022). Endocardium-to-coronary artery differentiation during heart development and regeneration involves sequential roles of Brmp2 and Cxcl12/Cxcr4. *Dev. Cell* 57, 2517–2532.e6. <https://doi.org/10.1016/j.devcel.2022.10.007>.
  37. Patra, C., Kontarakis, Z., Kaur, H., Rayrikar, A., Mukherjee, D., and Stainier, D.Y.R. (2017). The zebrafish ventricle: A hub of cardiac endothelial cells for in vitro cell behavior studies. *Sci. Rep.* 7, 2687. <https://doi.org/10.1038/s41598-017-02461-1>.
  38. Lawson, N.D., and Weinstein, B.M. (2002). In vivo imaging of embryonic vascular development using transgenic zebrafish. *Dev. Biol.* 248, 307–318. <https://doi.org/10.1006/dbio.2002.0711>.
  39. Asakawa, K., Suster, M.L., Mizusawa, K., Nagayoshi, S., Kotani, T., Urasaki, A., Kishimoto, Y., Hibi, M., and Kawakami, K. (2008). Genetic dissection of neural circuits by Tol2 transposon-mediated Gal4 gene and enhancer trapping in zebrafish. *Proc. Natl. Acad. Sci. USA* 105, 1255–1260. <https://doi.org/10.1073/pnas.0704963105>.
  40. Fukui, H., Terai, K., Nakajima, H., Chiba, A., Fukuhara, S., and Mochizuki, N. (2014). S1P-Yap1 signaling regulates endoderm formation required for cardiac precursor cell migration in zebrafish. *Dev. Cell* 31, 128–136. <https://doi.org/10.1016/j.devcel.2014.08.014>.
  41. Nakajima, H., Ishikawa, H., Yamamoto, T., Chiba, A., Fukui, H., Sako, K., Fukumoto, M., Mattonet, K., Kwon, H.-B., Hui, S.P., et al. (2023). Endoderm-derived islet1-expressing cells differentiate into endothelial cells to function as the vascular HSPC niche in zebrafish. *Dev. Cell* 58, 224–238.e7. <https://doi.org/10.1016/j.devcel.2022.12.013>.
  42. Matsuoka, R.L., Marass, M., Avdesh, A., Helker, S.M., Maischein, H.-M., Grosse, A.S., Kaur, H., Lawson, N.D., Herzog, W., et al. (2016). Radial glia regulate vascular patterning around the developing spinal cord. *eLife* 5, e20253. <https://doi.org/10.7554/eLife.20253.001>.
  43. Kawakami, K., Takeda, H., Kawakami, N., Kobayashi, M., Matsuda, N., and Mishina, M. (2004). A transposon-mediated gene trap approach identifies developmentally regulated genes in zebrafish. *Dev. Cell* 7, 133–144. <https://doi.org/10.1016/j.devcel.2004.06.005>.
  44. Asakawa, K., and Kawakami, K. (2009). The Tol2-mediated Gal4-UAS method for gene and enhancer trapping in zebrafish. *Methods* 49, 275–281. <https://doi.org/10.1016/j.ymeth.2009.01.004>.
  45. Pfeiffer, B.D., Truman, J.W., and Rubin, G.M. (2012). Using translational enhancers to increase transgene expression in *Drosophila*. *Proc. Natl. Acad. Sci. USA* 109, 6626–6631. <https://doi.org/10.1073/pnas.1204520109>.
  46. Schindelin, J., Arganda-Carreras, I., Frise, E., Kaynig, V., Longair, M., Pietzsch, T., Preibisch, S., Rueden, C., Saalfeld, S., Schmid, B., et al. (2012). Fiji: an open-source platform for biological-image analysis. *Nat. Methods* 9, 676–682. <https://doi.org/10.1038/nmeth.2019>.
  47. Hao, Y., Hao, S., Andersen-Nissen, E., Mauck, W.M., Zheng, S., Butler, A., Lee, M.J., Wilk, A.J., Darby, C., Zager, M., et al. (2021). Integrated analysis of multimodal single-cell data. *Cell* 184, 3573–3587.e29. <https://doi.org/10.1016/j.cell.2021.04.048>.
  48. Wolf, F.A., Angerer, P., and Theis, F.J. (2018). SCANPY: large-scale single-cell gene expression data analysis. *Genome Biol.* 19, 15. <https://doi.org/10.1186/s13059-017-1382-0>.
  49. McGinnis, C.S., Murrow, L.M., and Gartner, Z.J. (2019). DoubletFinder: doublet detection in single-cell RNA sequencing data using artificial nearest neighbors. *Cell Syst.* 8, 329–337.e4. <https://doi.org/10.1016/j.cels.2019.03.003>.
  50. Waskom, M. (2021). seaborn: statistical data visualization. *J. Open Source Softw.* 6, 3021. <https://doi.org/10.21105/joss.03021>.
  51. Urasaki, A., Morvan, G., and Kawakami, K. (2006). Functional dissection of the Tol2 transposable element identified the minimal cis-sequence and a highly repetitive sequence in the subterminal region essential for transposition. *Genetics* 174, 639–649. <https://doi.org/10.1534/genetics.106.060244>.
  52. Chung, J.H., Whiteley, M., and Felsenfeld, G. (1993). A 5' element of the chicken  $\beta$ -globin domain serves as an insulator in human erythroid cells and protects against position effect in *Drosophila*. *Cell* 74, 505–514. [https://doi.org/10.1016/0092-8674\(93\)80052-g](https://doi.org/10.1016/0092-8674(93)80052-g).
  53. Esengil, H., Chang, V., Mich, J.K., and Chen, J.K. (2007). Small-molecule regulation of zebrafish gene expression. *Nat. Chem. Biol.* 3, 154–155. <https://doi.org/10.1038/nchembio858>.
  54. Ando, K., Fukuhara, S., Izumi, N., Nakajima, H., Fukui, H., Kelsh, R.N., and Mochizuki, N. (2016). Clarification of mural cell coverage of vascular endothelial cells by live imaging of zebrafish. *Development* 143, 1328–1339. <https://doi.org/10.1242/dev.132654>.
  55. Sehnert, A.J., Huq, A., Weinstein, B.M., Walker, C., Fishman, M., and Stainier, D.Y.R. (2002). Cardiac troponin T is essential in sarcomere assembly and cardiac contractility. *Nat. Genet.* 31, 106–110. <https://doi.org/10.1038/ng875>.
  56. Curtin, E., Hickey, G., Kamel, G., Davidson, A.J., and Liao, E.C. (2011). Zebrafish *wnt9a* is expressed in pharyngeal ectoderm and is required for palate and lower jaw development. *Mech. Dev.* 128, 104–115. <https://doi.org/10.1016/j.mod.2010.11.003>.
  57. Oginuma, M., Nishida, M., Ohmura-Adachi, T., Abe, K., Ogamino, S., Mogi, C., Matsui, H., and Ishitani, T. (2022). Rapid reverse genetics systems for *Nothobranchius furzeri*, a suitable model organism to study vertebrate aging. *Sci. Rep.* 12, 11628. <https://doi.org/10.1038/s41598-022-15972-3>.

## STAR★METHODS

### KEY RESOURCES TABLE

REAGENT or RESOURCE	SOURCE	IDENTIFIER
<b>Antibodies</b>		
Mouse monoclonal anti-GFP	Clontech	Cat# 632569; RRID: AB_3662129
Rabbit polyclonal anti-RsRed	Clontech	Cat# 632496; RRID: AB_10013483
Mouse monoclonal anti-Troponin T (Cardiac Isoform)	Thermo Fisher Scientific	Cat# MS295P1; RRID: AB_61808
Anti-mouse Alexa Fluor 488 IgG	Thermo Fisher Scientific	Cat# A-11029; RRID: AB_2534088
Anti-rabbit Alexa Fluor 546 IgG	Thermo Fisher Scientific	Cat# A-11035; RRID: AB_2534093
Anti-mouse Alexa Fluor 546 IgG	Thermo Fisher Scientific	Cat# A-11030; RRID: AB_2534089
Sheep Anti-Mouse IgG – Horseradish Peroxidase	GE Healthcare	Cat# NA931; RRID: AB_772210
Anti-DIG-AP Fab fragments	Roche	Cat# 11093274910; RRID: AB_2734716
<b>Chemicals, peptides, and recombinant proteins</b>		
IWR-1-endo	Sigma-Aldrich	681669
LGK974	Cayman Chemical	14072
2,3-Butanedione 2-Monoxime	Sigma-Aldrich	B0753
Metronidazole	Sigma-Aldrich	M1547
5-ethynyl-2'-deoxyuridine	Tokyo Chemical Industry	E1057
Dimethyl Sulfoxide	FUJIFILM	045-24511
Tebufenozide	FUJIFILM	207-19041
Tricaine	Sigma-Aldrich	A5040
N-Phenylthiourea	Tokyo Chemical Industry	P0237
Low-melting agarose	Sigma-Aldrich	A9414
4',6-diamidino-2-phenylindole	Thermo Fisher Scientific	D1306
Collagenase type IV	Worthington	LS004188
<b>Critical commercial assays</b>		
pCR4-bluntTOPO	Thermo Fisher Scientific	451245
SMART-Seq v4 Ultra Low Input RNA Kit for Sequencing	Clontech	634888
NEBNext Ultra II Directional RNA Library Prep Kit for Illumina	New England Biolabs	E7760
SuperScript IV Reverse Transcriptase	Thermo Fisher Scientific	18090050
KOD SYBR qPCR Mix	TOYOBO	QKD-201
DIG RNA labeling kit	Sigma-Aldrich	11175025910
SYTOX blue	Thermo Fisher Scientific	S34857
Click-iT EdU Cell Proliferation Kit for Imaging, Alexa Fluor 647 dye	Thermo Fisher Scientific	C10340
RNAscope Multiplex Fluorescent Reagent Kit v2	ACDbio	323100
Alt-R CRISPR-Cas9 tracrRNA	IDT	1072532
Alt-R S.p. Cas9 Nuclease V3	IDT	1081058
Chromium Next GEM single cell 3'reagent kits v3.1	10x GENOMICS	1000128
<b>Deposited data</b>		
Raw and analyzed data	This paper	GEO: GSE223462
<b>Experimental models: Organisms/strains</b>		
Zebrafish: wild-type AB	Zebrafish International Resource Center (ZIRC)	ZFIN: ZDB-GENO-960809-7

(Continued on next page)

**Continued**

REAGENT or RESOURCE	SOURCE	IDENTIFIER
Zebrafish: <i>Tg(fli1:EGFP)<sup>y1</sup></i>	Lawson and Weinstein <sup>38</sup>	ZFIN: ZDB-ALT-011017-8
Zebrafish: <i>Tg(UAS:EGFP)<sup>nkuasgfp1a</sup></i>	Asakawa et al. <sup>39</sup>	ZDB-ALT-080528-1
Zebrafish: <i>Tg(BRE:EGFP)<sup>mw29</sup></i>	ZIRC; Collery and Link <sup>20</sup>	ZFIN: ZDB-ALT-110308-1
Zebrafish: <i>Tg(myl7:NLS-mCherry)<sup>ncv11</sup></i>	Fukui et al. <sup>40</sup>	ZFIN: ZDB-ALT-150218-2
Zebrafish: <i>Tg(fli1:mCherry)<sup>ncv501</sup></i>	Nakajima et al. <sup>41</sup>	N/A
Zebrafish: <i>Tg(kdrl:TagBFP)<sup>mu293</sup></i>	Matsuoka et al. <sup>42</sup>	ZFIN: ZIALT-170119-12
Zebrafish: <i>Tg(fli1:GAL4db-Hsa.TCF7L2<math>\Delta</math>C-2A-mCherry)<sup>ncv15</sup></i>	Kashiwada et al. <sup>14</sup>	ZFIN: ZDB-ALT-150313-3
Zebrafish: <i>Tg(Hsa.DLL4:EGFP)<sup>ncv513</sup></i>	This paper	N/A
Zebrafish: <i>Tg(actb2:GAL4db-Hsa.TCF7L2<math>\Delta</math>C-2A-mCherry)<sup>ncv538</sup></i>	This paper	N/A
Zebrafish: <i>Tg(myl7:GAL4db-Hsa.TCF7L2<math>\Delta</math>C-2A-mCherry)<sup>ncv539</sup></i>	This paper	N/A
Zebrafish: <i>Tg(myl7:GAL4db-Hsa.TCF7L2<math>\Delta</math>C,cryaa:EGFP)<sup>ncv82</sup></i>	This paper	N/A
Zebrafish: <i>Tg(myl7:GAL4-VP16-Bmo.Ecr)<sup>ncv77</sup></i>	This paper	N/A
Zebrafish: <i>Tg(5xUAS:NTR-mCherry)<sup>ncv84</sup></i>	This paper	N/A
Zebrafish: <i>Tg(5xUAS:tcf7l1a<math>\Delta</math>N-mCherry)<sup>ncv540</sup></i>	This paper	N/A
Zebrafish: <i>Tg(5xUAS:dEGFP)<sup>ncv549</sup></i>	This paper	N/A
Zebrafish: <i>Tg(5xUAS:tagBFP-P2A-NTR2.0)<sup>ncv551</sup></i>	This paper	N/A
Zebrafish: <i>TgBAC(tbx2b:EGFP)<sup>ncv83</sup></i>	This paper	N/A
Zebrafish: <i>TgBAC(tbx2b:GAL4FF)<sup>ncv542</sup></i>	This paper	N/A
Zebrafish: <i>TgBAC(esm1:dEGFP)<sup>ncv543</sup></i>	This paper	N/A
<b>Oligonucleotides</b>		
See <a href="#">Table S3</a> for Morpholinos	Gene Tools	N/A
See <a href="#">Table S3</a> for CRISPR-Cas9 crRNAs	IDT	N/A
See <a href="#">Table S3</a> for primers	Fasmac	N/A
<b>Recombinant DNA</b>		
Plasmid: pTol2	Kawakami et al. <sup>43</sup>	N/A
Plasmid: T2MUASMCS	Asakawa and Kawakami <sup>44</sup>	ZFIN: ZDB-TGCONSTRCT-100914-4
Plasmid: 5xUAS:GAP-EGFP-P2A-NfsB_Vv F70A/F108Y,he:tagBFP2	Addgene; Sharrock et al. <sup>32</sup>	158652
Plasmid: pJFRC81-10XUAS-IVS-Syn21-GFP-p10	Addgene; Pfeiffer et al. <sup>45</sup>	36432
Plasmid: pTol2-actb2-GAL4db-Hsa.TCF7L2 $\Delta$ C-2A-mCherry	This paper	N/A
Plasmid: pTol2-myl7-GAL4db-Hsa.TCF7L2 $\Delta$ C-2A-mCherry	This paper	N/A
Plasmid: pTol2-cryaa-EGFP-HS4-myl7-GAL4db-Hsa.TCF7L2 $\Delta$ C	This paper	N/A
Plasmid: pTol2-myl7-GAL4-VP16-Bmo.Ecr	This paper	N/A
Plasmid: pT2A-UAS-NTR-mCherry	This paper	N/A
Plasmid: pT2A-UAS-Tcf7l1a $\Delta$ N-mCherry	This paper	N/A
Plasmid: tbx2b BAC:EGFP	This paper	N/A
Plasmid: tbx2b BAC:GAL4FF	This paper	N/A
Plasmid: esm1 BAC:dEGFP	This paper	N/A
<b>Software and algorithms</b>		
Imaris	Oxford Instruments	RRID: SCR_007370

(Continued on next page)

**Continued**

REAGENT or RESOURCE	SOURCE	IDENTIFIER
FV10-ASW	Olympus	RRID: SCR_014215
Fiji	Schindelin et al. <sup>46</sup>	RRID: SCR_002285
Cell Ranger	10X Genomics	RRID: SCR_017344
Seurat	Hao et al. <sup>47</sup>	RRID: SCR_016341
Scanpy	Wolf et al. <sup>48</sup>	RRID: SCR_018139
DoubletFinder	McGinnis et al. <sup>49</sup>	RRID: SCR_018771
CLC Genomics Workbench	QIAGEN	RRID: SCR_011853
SciPy	The SciPy community	RRID: SCR_008058
Seaborn	Waskom <sup>50</sup>	RRID: SCR_018132

**EXPERIMENTAL MODEL AND SUBJECT DETAILS**

**Animal studies**

Zebrafish (*Danio rerio*) were maintained and bred in 28 °C water (pH 7.25 and conductivity 500  $\mu$ S) with a 14 h on/10 h off light cycle. Embryos and larvae were incubated in the E3 medium at 28 °C. For confocal imaging, zebrafish embryos and larvae were dechorionated and anesthetized in 0.016% tricaine (Sigma-Aldrich, A5040) in the E3 medium. For heart resection, zebrafish were anesthetized in 0.016% tricaine in fish water. Animal experiments were approved by the institutional animal committee of the National Cerebral and Cardiovascular Center and performed according to the guidelines of the institute (Permit number: 22054) that follow the national (Japan) ethical and animal welfare regulations.

The fish lines used in this study were: AB as a wild-type line, *Tg(5xUAS:EGFP)<sup>nkuasgfp1a</sup>*, *Tg(myl7:NLS-mCherry)<sup>ncv11</sup>*, *Tg(BRE:EGFP)<sup>mw29</sup>*, *Tg(fli1:EGFP)<sup>y1</sup>*, *Tg(fli1:mCherry)<sup>ncv501</sup>*, *Tg(kdr:TagBFP)<sup>mu293</sup>*, *Tg(fli1:GAL4db-Hsa.TCF7L2 $\Delta$ C-2A-mCherry)<sup>ncv15</sup>*, *Tg(actb2:GAL4db-Hsa.TCF7L2 $\Delta$ C-2A-mCherry)<sup>ncv538</sup>*, *Tg(Hsa.DLL4:EGFP)<sup>ncv513</sup>*, *Tg(myl7:GAL4db-Hsa.TCF7L2 $\Delta$ C-2A-mCherry)<sup>ncv539</sup>*, *Tg(myl7:GAL4db-Hsa.TCF7L2 $\Delta$ C,cryaa:EGFP)<sup>ncv82</sup>*, *Tg(myl7:GAL4-VP16-Bmo.Ecr)<sup>ncv77</sup>*, *Tg(5xUAS:NTR-mCherry)<sup>ncv84</sup>*, *Tg(5xUAS:tcf7l1a $\Delta$ N-mCherry)<sup>ncv540</sup>*, *Tg(5xUAS:dEGFP)<sup>ncv549</sup>*, *Tg(5xUAS:tagBFP-P2A-NTR2.0)<sup>ncv551</sup>*, *TgBAC(tbx2b:EGFP)<sup>ncv83</sup>*, *TgBAC(tbx2b:GAL4FF)<sup>ncv542</sup>*, and *TgBAC(esm1:dEGFP)<sup>ncv543</sup>*. Both males and females were used in this study.

**METHOD DETAILS**

**Plasmids**

The Tol2 vector system was kindly provided by K. Kawakami (National Institute of Genetics, Japan).<sup>51,43</sup> The Tol2\_amp plasmid and the pCS2\_GAL4FF\_KanR plasmid for BAC recombineering were kindly provided by S. Schulte-Merker (University of Münster, Germany).

To construct the pTol2-actb2 vector, a promoter/enhancer sequence of the zebrafish *actb2* gene obtained by PCR was inserted into the pTol2 vector.<sup>43</sup> Primers to amplify the *actb2* promoter were as follows: Mull-*actb2*-forward, 5'-acgcgtCAAGCCTGAGTATCTGCACCATC-3'; Spel-*actb2*-reverse, 5'-actagtGGCTGAACTGTAAAAGAAAGGGA-3'. To construct the pTol2-actb2-GAL4db-Hsa.TCF7L2 $\Delta$ C-2A-mCherry plasmid, a cDNA fragment encoding the GAL4-DNA-binding domain (GAL4db) fused to human TCF7L2 lacking the carboxy-terminus (amino acids 1–314) followed by 2A peptide and mCherry (GAL4db-Hsa.TCF7L2 $\Delta$ C-2A-mCherry) from pcDNA3.1-GAL4db-Hsa.TCF7L2 $\Delta$ C-2A-mCherry<sup>14</sup> was inserted into the pTol2-actb2 vector.

To construct the Tol2-myl7-GAL4db-Hsa.TCF7L2 $\Delta$ C-2A-mCherry plasmid, a GAL4db-Hsa.TCF7L2 $\Delta$ C-2A-mCherry fragment was inserted into the pTol2-myl7 vector.<sup>40</sup> To construct the pTol2-cryaa-EGFP-HS4-myl7-GAL4db-Hsa.TCF7L2 $\Delta$ C plasmid, a promoter/enhancer sequence of the *cryaa* gene obtained by PCR, an EGFP fragment derived from pEGFP-N1 (Clontech), a  $\beta$ -globin insulator (hs4) derived from pJC13-1,<sup>52</sup> *myl7* promoter, and a GAL4db-Hsa.TCF7L2 $\Delta$ C fragment obtained by PCR were inserted into the pTol2 vector. Primers to amplify the *cryaa* promoter were as follows: PspOMI-*cryaa*-forward, 5'-aaGGGCCCGattggcgatctctacttagc-3'; NheI-*cryaa*-reverse, 5'-agGCTAGCaatgtcagacctgtaactccttac-3'.

To construct the pTol2-myl7-GAL4-VP16-Bmo.Ecr plasmid, a DNA fragment encoding GAL4 fused to VP16 and *Bombyx mori* ecdysone receptor (GAL4-VP16-Bmo.Ecr) derived from pCS2-GR Ecr-F<sup>53</sup> was inserted into the pTol2-myl7 vector.

To construct the pmCherry-NTR plasmid, a DNA fragment encoding NTR derived from pcDNA-NTR, a gift from D.Y. Stainier (Max Planck Institute), was inserted into the pmCherry-N1 (Clontech). To construct the pT2A-UAS-NTR-mCherry plasmid, a DNA fragment encoding NTR fused to mCherry derived from the pmCherry-NTR was inserted into the T2MUASMCS vector.<sup>44</sup>

To construct pmCherry-Tcf7l1a $\Delta$ N, a cDNA fragment encoding zebrafish Tcf7l1a lacking the  $\beta$ -catenin binding domain (amino acids 55–561) derived from pTol1-14XUAS-zTcf3-delta N-EGFP<sup>14</sup> was inserted into pmCherry-N1. To construct pT2A-UAS-Tcf7l1a $\Delta$ N-mCherry, a DNA fragment encoding Tcf7l1a $\Delta$ N fused to mCherry derived from pmCherry-Tcf7l1a $\Delta$ N was inserted into the T2MUASMCS vector.

To construct pT2A-UAS-dEGFP, a DNA fragment encoding dEGFP derived from pTols-14xUAS-dEGFP was inserted into the T2MUASMCS vector.

To construct pT2A-UAS-NTR2.0-P2A-TagBFP, the deG sequence of the pT2A-UAS-IVS-syn21-deG-p10 vector was replaced by a DNA fragment encoding NTR2.0-P2A-TagBFP derived from pME-NTR2.0-P2A-TagBFP. NTR2.0 was originally subcloned from 5xUAS:GAP-EGFP-P2A-NfsB\_Vv F70A/F108Y,he:tagBFP2.<sup>32</sup> pT2A-UAS-IVS-syn21-deG-p10 was constructed by inserting a translational enhancing element (IVS-Syn21) and p10 polyA from pJFRC81-10XUAS-IVS-Syn21-GFP-p10<sup>45</sup> and the dEGFP fragment into the T2MUASMCS vector. 5xUAS:GAP-EGFP-P2A-NfsB\_Vv F70A/F108Y,he:tagBFP2 was a gift from Jeff Mumm (Addgene plasmid # 158652; <http://n2t.net/addgene:158652>; RRID:Addgene\_158652). pJFRC81-10XUAS-IVS-Syn21-GFP-p10 was a gift from Gerald Rubin (Addgene plasmid # 36432; <http://n2t.net/addgene:36432>; RRID:Addgene\_36432).

### BAC recombineering

The pRedET plasmid (GeneBridge) was introduced into *E. coli* containing the CH73-142M16 and CH73-139N10 BAC clones encoding the *tbx2b* gene and *esm1* genes, respectively (BacPAC resources), by electroporation (1800 V, 25  $\mu$ F, 200  $\Omega$ ). The DNA fragment encoding two tol2 sequences with an ampicillin resistance cassette was amplified by PCR using Tol2\_amp as a template and was inserted into BAC vectors. The cDNA fragment encoding either EGFP, GAL4FF, or dEGFP together with a kanamycin resistance cassette was amplified by PCR using pCS2\_EGFP\_KanR,<sup>54</sup> pCS2\_GAL4FF\_KanR, or pCS2\_dEGFP\_KanR<sup>41</sup> as a template, respectively, and was inserted into the start ATG of the *tbx2b* gene or *esm1* gene. Primers for amplification of EGFP\_KanR or GAL4FF\_KanR for *tbx2b* gene were as follows: *tbx2b*\_EGFP\_forward, 5'-agccagagaacacacctctaaatatactcttctactactggttggatgcaACCATGGTGAGCAAGGGCGAGGAG-3'; *tbx2b*\_GAL4FF\_forward, 5'-agccagagaacacacctctaaatatactcttctactactggttggatgcaACCATGAAGCTACTGTCTTCTATCGAAC-3'; *tbx2b*\_KanR\_reverse, 5'-gcgtggaaaggtgtaagccatcgcagtcctctgtaaaaactggatctctTCAGAAGAACTCGTCAA GAAGGCG-3'. Primers to amplify the dEGFP\_KanR for the *esm1* gene were as follows: *esm1*\_dEGFP\_forward, 5'-tcctcccaacactg cagaccgaagatcgatccaaccgcccgttgcacACCATGGTGAGCAAGGGCGAG; *esm1*\_KanR\_reverse, 5'-gtctcccaaaaaccaccatcag tacgaacatcaggatggcaaacacacgTCAGAAGAACTCGTCAAGAAGGCG-3'.

### Transgenic zebrafish lines

We used the following previously published zebrafish lines: *Tg(5xUAS:EGFP)<sup>nkuasgfp1a</sup>*,<sup>39</sup> *Tg(myf7:NLS-mCherry)<sup>ncv11</sup>*,<sup>40</sup> *Tg(BRE:EGFP)<sup>mw29</sup>*,<sup>20</sup> and *Tg(fli1:EGFP)<sup>y1</sup>*,<sup>38</sup> *Tg(fli1:mCherry)<sup>ncv501</sup>*,<sup>41</sup> *Tg(kdrl:TagBFP)<sup>mu293</sup>*,<sup>42</sup> *Tg(fli1:GAL4db-Hsa.TCF7L2 $\Delta$ C-2A-mCherry)<sup>ncv15</sup>*,<sup>14</sup> *Tg(Hsa.DLL4:EGFP)<sup>ncv513</sup>* was provided by S. Fukuhara and S. Yuge (Nippon Med. School). The following zebrafish lines were established by injecting transposase mRNA (25 pg) and either Tol2-based plasmids (30 pg) or DNA (100 pg) into one-cell stage either AB or *Tg(5xUAS:EGFP)<sup>nkuasgfp1a</sup>* embryos; *Tg(actb2:GAL4db-Hsa.TCF7L2 $\Delta$ C-2A-mCherry)<sup>ncv538</sup>*, *Tg(myf7:GAL4db-Hsa.TCF7L2 $\Delta$ C-2A-mCherry)<sup>ncv539</sup>*, *Tg(myf7:GAL4db-Hsa.TCF7L2 $\Delta$ C,cryaa:EGFP)<sup>ncv82</sup>*, *Tg(myf7:GAL4-VP16-Bmo.Ecr)<sup>ncv77</sup>*, *Tg(5xUAS:NTR-mCherry)<sup>ncv84</sup>*, *Tg(5xUAS:tcf7l1a $\Delta$ N-mCherry)<sup>ncv540</sup>*, *Tg(5xUAS:dEGFP)<sup>ncv549</sup>*, *Tg(5xUAS:tagBFP-P2A-NTR2.0)<sup>ncv551</sup>*, *TgBAC(tbx2b:EGFP)<sup>ncv83</sup>*, *TgBAC(tbx2b:GAL4FF)<sup>ncv542</sup>*, and *TgBAC(esm1:dEGFP)<sup>ncv543</sup>*. Tol2 transposase mRNAs were *in vitro* transcribed with SP6 RNA polymerase from the linearized pCS2-TP vector using the mMMESSAGE mMACHINE kit (Thermo Fisher Scientific, AM1340). Throughout the text, all Tg lines used in this study are simply described without their line numbers. Hsa.DLL4, Hsa.TCF7L2 $\Delta$ C, tcf7l1a $\Delta$ N, and GAL4-VP16-Bmo.Ecr have been abbreviated to DLL4, TCF $\Delta$ C, TCF $\Delta$ N, and GvEcr, respectively. For example, *Tg(myf7:GAL4-VP16-Bmo.Ecr)<sup>ncv77</sup>* is abbreviated to *Tg(myf7:GvEcr)*. In addition, *cryaa:EGFP* is omitted throughout the main text: *Tg(myf7:GAL4db-Hsa.TCF7L2 $\Delta$ C,cryaa:EGFP)<sup>ncv82</sup>* is written as *Tg(myf7:GAL4db-TCF $\Delta$ C)*.

### Genotyping

To examine the genotype of *Tg(UAS:EGFP)* or *Tg(5xUAS:dEGFP)* fish, *EGFP* was amplified using genomic DNA extracted from embryos after imaging.

To examine the genotype of *Tg(myf7:GAL4db-TCF7 $\Delta$ C-2A-mCherry)* fish crossed with *Tg(myf7:NLS-mCherry)*, *GAL4* was amplified using genomic DNA extracted from embryos after imaging.

To examine the genotype of *Tg(myf7:GvEcr)*; *Tg(5xUAS:TCF $\Delta$ N-mCherry)*, *GAL4*, and *mCherry* were amplified using genomic DNA extracted from the tail. *GAL4* and *mCherry* double negative fish were used as control fish.

To examine the genotype of *Tg(fli1:EGFP)*; *Tg(myf7:GAL4db-TCF7 $\Delta$ C,cryaa:EGFP)*; *Tg(5xUAS:NTR-mCherry)* fish, *fli1:EGFP* in blood vessels, *cryaa:EGFP* in the lens, and *UAS:NTR-mCherry* in the atrioventricular canal (AVC) were observed at 4 dpf using fluorescence stereo microscope. The *fli1:EGFP*<sup>+</sup>, *cryaa:EGFP*<sup>+</sup>, *UAS:NTR-mCherry*<sup>-</sup> fish were used as controls.

To examine the genotype of *Tg(fli1:EGFP)*; *TgBAC(tbx2b:EGFP)*; *Tg(5xUAS:NTR-mCherry)* fish, *fli1:EGFP* in blood vessels and *UAS:NTR-mCherry* at the AVC were observed at 4 dpf using fluorescence stereo microscope. The *fli1:EGFP*<sup>+</sup>, *UAS:NTR-mCherry*<sup>-</sup> fish were used as controls.

To examine the genotype of *Tg(fli1:mCherry)*; *Tg(DLL4:EGFP)*; *Tg(myf7:GAL4db-TCF7 $\Delta$ C,cryaa:EGFP)*; *Tg(5xUAS:tagBFP-P2A-NTR2.0)* fish, *fli1:mCherry* in blood vessels, *DLL4:EGFP* in arteries, *cryaa:EGFP* in the lens, and *UAS:tagBFP-P2A-NTR2.0* at the AVC were observed at 4 dpf using fluorescence stereo microscope. The *fli1:mCherry*<sup>+</sup>, *DLL4:EGFP*<sup>+</sup>, *cryaa:EGFP*<sup>-</sup>, and *UAS:tagBFP-P2A-NTR2.0*<sup>-</sup> fish were used as controls.

The primer sequences used for genotyping are listed in Table S3.

### Microinjection of oligonucleotide

We injected the following morpholino oligonucleotides (MOs) (Gene Tools): *tnnt2a* atg-MO (2 ng, 5'-CATGTTTGCTCTGATCTGACACGCA-3'),<sup>55</sup> *wnt2bb* MO (5 ng, 5'-GTGTGCCATATAAAAGTATTCCCCG-3'),<sup>23</sup> *wnt9b* MO (2 ng, 5'-CAGTCCCTCGGAAGCCCGGTGCACAT-3'),<sup>56</sup> and control MO (5'-CCTCTTACCTCAGTTACAATTTATA-3'). We injected the MO into embryos at the one-cell stage. The control group was injected with the same amount of the control MO as the experimental group.

The triple-target CRISPR-mediated F0 mutant<sup>57</sup> was generated by the sgRNA (IDT) targeting the following sequence: 5'-CCTGTCCGCTGCGACTTATTGCC-3', 5'-CCAACGAGCCTACAAACGGTAAA-3', 5'-CCTCGAGTGCCGCTACCAGTTCC-3'. The preparation of RNP complex was prepared according to the manufacturer's instructions, except that 3  $\mu$ l of each crRNA was used to prepare the gRNA solution.

### Chemical treatment

Fish were treated with the following chemicals: metronidazole (MTZ, 5 mM, Sigma-Aldrich, M1547) dissolved in fish water containing dimethyl sulfoxide (DMSO, 0.2%, FUJIFILM, 045-24511) immediately before treatment, to induce the ablation of NTR-expressing cells; tebufenozide (TBF, 20  $\mu$ M, FUJIFILM, 207-19041) to induce cardiomyocyte-specific (CM-specific) expression driven by *Tg(myf7:GvEcR)*; IWR1-endo (IWR1, 10  $\mu$ M, Sigma-Aldrich, 681669), a tankyrase inhibitor, to inhibit Wnt/ $\beta$ -catenin signaling; LGK974 (20  $\mu$ M, Cayman Chemical, 14072), a porcupine inhibitor, to inhibit Wnt ligand secretion; 2,3-butanedione 2-monoxime (BDM, 30 mM, Sigma-Aldrich, B0753) to induce cardiac arrest; 5-ethynyl-2'-deoxyuridine (EdU, 1 mM, Tokyo Chemical Industry, E1057) to detect proliferating cells; DMSO as a control.

Embryos and larvae were treated with drugs dissolved in the E3 medium and incubated at 28 °C.

Juvenile and adult fish were treated with drugs dissolved in fish water in the dark. After exposure to the chemicals, the water was changed to remove the drug, and the fish were kept in the tank without water circulation. Either MTZ or TBF was treated for 12 h every 2 days. In [Figure S3O](#), IWR1 was treated for 12 h every day. In [Figure S4](#), IWR1 was treated for 48 h.

### Imaging

To obtain images of embryos and larvae without pigmentation, a 0.2 mM solution of N-phenylthiourea (PTU) (Tokyo Chemical Industry, P0237) was added to the E3 medium from 24 hpf. Embryos and larvae were anesthetized with 0.1 mg/ml of tricaine (Sigma-Aldrich, A5040) and then mounted in 1.5% low-melting agarose (Sigma-Aldrich, A9414). To observe the heart, anesthetized embryos and larvae were treated with 30 mM BDM and then mounted in 1.5% low-melting agarose containing the same concentration of tricaine and BDM as the medium.

For observation of coronary vessels (CVs), zebrafish hearts were dissected and fixed in 4% paraformaldehyde (PFA) overnight at 4 °C. Hearts were washed in phosphate-buffered saline (PBS) and embedded in 1.5% low-melting agarose.

To observe CVs of *ex vivo* culture, hearts were resected from *Tg(fli1:EGFP)* at 1-month-old. The resected hearts were collected in 35 mm dishes containing Hanks' balanced salt solution (HBSS) without calcium and magnesium (Thermo Fisher Scientific, 14175095), removed atrium, and transferred to the glass-based dish (IWAKI, 3910-035) containing L-15 medium (Thermo Fisher Scientific, 21083027) with 10% FBS, streptomycin, and penicillin. To avoid rolling the hearts, 70% of the groove of the dish was covered with cover glass (MATSUNAMI, 2-176-01).

To observe DLL4:EGFP<sup>+</sup> CVs, hearts were imaged in the same manner as *ex vivo* culture hearts. The only difference was the treatment with 30 mM BDM during imaging.

Confocal imaging was performed using an FV1000 confocal microscope (Olympus), an FV1200 confocal microscope (Olympus), and an FV3000 confocal microscope (Olympus). We used either a 20x water immersion objective (Olympus XLUMPlan FL\_N, 1.0 N.A.) or a 10x water immersion objective (Olympus UPlanFL N). All confocal images were processed and analyzed with Imaris 9.8.0, 9.9.1, or 10.0.0 software (Oxford Instruments).

Stereomicroscopic images of *in situ* hybridization samples and alcian blue-stained samples were taken using an SZX16 stereo microscope (Olympus) with an Olympus DP2-BSW camera and CellSens imaging software (Olympus).

### Sectioning of zebrafish hearts

For cryosection, hearts were excised and fixed with 4% PFA overnight at 4 °C. After washing with PBS, the hearts were immersed in 30% sucrose/PBS overnight at 4 °C. The hearts were then embedded in the Tissue-Tek OCT compound (Sakura, 4583) and frozen. The frozen blocks were sectioned into 10  $\mu$ m thick sections with a microtome (Leica, RM2125RT).

### Immunohistochemistry (IHC)

Tissue sections were fixed with 4% PFA, permeabilized with 0.3% Triton X-100 at room temperature (RT) for 10 min, and blocked with PBS containing 10% normal goat serum at RT for 1 h. The sections were immunostained with mouse anti-GFP (1:200, Clontech, 632569), rabbit anti-DsRed (1:200, Clontech, 632496), or mouse anti-Troponin T (1:200, Thermo Fisher Scientific, MS295P1) antibodies at 4 °C overnight and visualized with secondary antibodies, anti-mouse Alexa Fluor 488 IgG (1:300, Thermo Fisher Scientific, A-11029), anti-mouse Alexa Fluor 546 IgG (1:300, Thermo Fisher Scientific, A-11030), or anti-rabbit Alexa Fluor 546 IgG (1:300, Thermo Fisher Scientific, A-11035). 4',6-Diamidino-2-phenylindole (DAPI, 1:1,000, Thermo Fisher Scientific, D1306) was used to counterstain nuclei. Control experiments were performed by omitting the primary antibodies from the immunostaining procedure.

### EdU staining

Ventricles were removed from the hearts of EdU-treated fish, washed with 3%BSA/PBS, permeabilized with 0.5% Triton X-100 for 20 min at RT, and washed with 3%BSA/PBS. EdU was detected using the Click-iT™ EdU Cell Proliferation Kit for Imaging, Alexa Fluor™ 647 dye according to the manufacturer's instruction.

### *in situ* hybridization (ISH)

Plasmids for *myl7*, *tbx2b*, *wnt2bb*, *wnt9b*, *cp*, and *plvabp* probes were amplified from 24 hpf zebrafish cDNA library using the primer sequences in [Table S3](#) and cloned into the pCR4 Blunt TOPO vector (Thermo Fisher Scientific, 451245). Antisense probes labeled with digoxigenin (DIG) were prepared using an RNA labeling kit (Sigma-Aldrich, 11175025910). For whole-mount ISH, embryos and hearts were fixed in 4% PFA in PBS, dehydrated in methanol, and gradually rehydrated into PBS containing 0.1% Tween-20 (PBS-T). After digestion with PBS-T containing proteinase K for 30 min, embryos and hearts were fixed in 4% PFA and hybridized with antisense RNA probes in hybridization buffer (5 x SSC, 50% formamide, 5 mM EDTA, 0.1% Tween-20, 50  $\mu$ g/ml heparin, and 1 mg/ml Torula RNA) at 70°C overnight. After hybridization, embryos and larvae were washed with wash buffer A (75% formamide, 2xSSC) for 10 min at 70°C, wash buffer B (50% formamide, 2xSSC) for 10 min at 70°C, wash buffer C (25% formamide, 2xSSC) for 10 min at 70°C, wash buffer D (2xSSC) for 10 min at 70°C, twice wash buffer E (0.2xSSC) for 30 min at 65°C, and wash buffer F (0.1xSSC/PBS-T) for 5 min at RT, and PBS-T for 5 min at RT. Embryos and hearts were washed with MAB (0.1 M maleic acid, 0.15 M NaCl, pH 7.5) for 15 min at RT, blocked with blocking buffer (2% blocking reagent, Merck, 11096176001, 5% sheep serum in MAB) for 90 min, and incubated with anti-DIG antibody conjugated with alkaline phosphatase (Merck, 11093274910) in blocking buffer (1:5,000) at 4°C overnight. Embryos and hearts were rinsed twice with PBS-T, washed four times with PBS-T for 20 min at RT, and washed three times with staining buffer (0.1 M NaCl, 50 mM MgCl<sub>2</sub>, 0.1 M Tris-HCl, 0.1% Tween-20, pH 9.5) at RT. The colorimetric reaction was performed using BM purple (Merck, 11442074001). To stop the reaction, embryos were washed with PBS-T, fixed with 4% PFA at RT, and immersed in glycerol.

### RNAscope assay

RNAscope analysis of cryosections was performed using the RNAscope Multiplex Fluorescent Reagent Kit v2 (ACDbio, 323110) according to the manufacturer's instructions. The following probes were used for hybridization: *axin2*-C1 probe (ACDbio, 465351), *wnt2bb*-C2 probe (831171-C2), and *wnt9b*-C1 probe (ACDbio,504431). ISH signals were detected using Opal690 (AKOYA biosciences, FP1497001KT). After probe hybridization, sections were immunostained with anti-Troponin T antibody and horseradish peroxidase-conjugated anti-mouse gG (GE Healthcare, NA931) according to the protocols provided by ACDbio. IHC signals were detected using Opal520 (AKOYA biosciences, FP1487001KT).

### Alcian blue staining

Larvae were fixed with 4% PFA, stained with 0.02% Alcian Blue 8GX in 70% ethanol containing 80 mM MgCl<sub>2</sub> at RT overnight, rehydrated in water, bleached in 1.5% hydrogen peroxide in 1% KOH for 30 min, and stored in 50% glycerol in 0.25% KOH.

### Tissue clearing

Tissue clearing was performed with clear, unobstructed brain/body imaging cocktails and computational analysis reagent-1A (CUBIC-1A) {10% Triton X-100, 5% N,N,N',N'-tetrakis(2-hydroxypropyl)ethylenediamine, 10% urea, 25 mM NaCl} according to the modified methods on the RIKEN website (<http://cubic.riken.jp/>). Fixed hearts embedded in low-melting agarose gel were incubated in 1/2-diluted CUBIC-1A for 6 h at RT, CUBIC-1A overnight at RT, and CUBIC-1A for 1 week at 37 °C. During the incubation, we exchanged CUBIC-1A every day.

### Cell sorting

For RNA-seq, the AVC was resected from *Tg(myl7:GAL4db-TCFΔC-2A-mCherry);Tg(UAS:EGFP);Tg(myl7:NLS-mCherry)* hearts at 4~8 months. For scRNA-seq, hearts were resected from *Tg(fli1:EGFP);Tg(myl7:GAL4db-TCFΔC);(5xUAS:NTR-mCherry)* fish at 2.5 months treated with either DMSO (n = 15) or 5 mM MTZ (n = 15) for 30 days. For qPCR, hearts were resected from *Tg(fli1:EGFP);Tg(myl7:GAL4db-TCFΔC);(5xUAS:NTR-mCherry)* fish at 2.5 months or control fish treated with 5 mM MTZ for 30 days. The resected hearts were collected in 35 mm dishes containing HBSS without calcium and magnesium. The hearts were torn and were transferred to a 12-well plate. The hearts were digested with 3 mg/ml collagenase type IV (Worthington, LS004188)/HBSS for 30 min at 28.5 °C. After pipetting, the cells were collected into low-binding tubes, washed with 0.5% FBS/DMEM, and resuspended in 0.5% FBS/DMEM containing SYTOX blue dead cell stain (Thermo Fisher Scientific, S34857). Cells were sorted using either a FACSAria III cell sorter (BD Bioscience, for qPCR and RNA-seq) or a FACSFusion cell sorter (BD Bioscience, for scRNA-seq).

### RNA sequencing (RNA-seq)

Total RNAs were prepared from  $\beta$ -cat ON (mCherry<sup>+</sup> EGFP<sup>+</sup>) CMs and  $\beta$ -cat OFF (mCherry<sup>+</sup> EGFP<sup>-</sup>) CMs using a NucleoSpin XS kit (Macherey-Nagel, 740902.50) according to the manufacturer's instruction. Reverse transcription and cDNA library preparation were performed with a SMART-Seq v4 Ultra Low Input RNA Kit for Sequencing (Clontech, 634888). cDNA was fragmented with a Covaris S 220 instrument (Covaris). Libraries for RNA-seq were prepared using a NEBNext Ultra II Directional RNA Library Prep Kit for Illumina

(New England Biolabs, E7760) and sequenced on the NextSeq500 (Illumina) as 75 bp single-end reads. Over 14 million raw reads were generated per sample. The resulting RNA-seq data were analyzed using the CLC genomics workbench v.20.0.4 (Qiagen) according to the manufacturer's instructions. Trimmed and filtered reads were aligned to the zebrafish genome (GRCz 11.99). Differentially expressed genes (DEGs) in  $\beta$ -cat ON CMs were defined as those with >2.0-fold change and false discovery rate (FDR) <0.05 using iDEP.96 (<http://bioinformatics.sdstate.edu/idep96/>). GO analysis of DEGs was performed using DAVID (<https://david.ncifcrf.gov/>).

### single-cell RNA sequencing (scRNA-seq)

For the analysis of AVC cells, *Tg(fli1:EGFP);Tg(myf7:GAL4db-TCF $\Delta$ C);(5xUAS:NTR-mCherry)* fish at 1 month were treated with either DMSO ( $n = 25$ ) or 10  $\mu$ M IWR1 ( $n = 25$ ) for 48 h. The resected hearts were collected in 35 mm dishes containing HBSS without calcium and magnesium. The atrium and the ventricle were removed from AVCs. Only AVCs were transferred to a 12-well plate. The digestion procedure was the same as for cell sorting.

Sorted EGFP<sup>+</sup> cells or digested AVC cells were counted by a cell counter (Thermo Fisher Scientific) using trypan blue. The resulting endothelial cell suspension was loaded onto a 10X Chromium Controller (10X Genomics) according to the manufacturer's protocol. The scRNA-seq library was prepared using Chromium Next GEM single cell 3' reagent kits v3.1 (10X Genomics, 1000128), according to the manufacturer's protocol. Following droplet generation and barcoding, cDNA was synthesized and amplified. The cDNA was processed to construct Illumina sequencing libraries. Sequencing was performed on a NextSeq 500 (Illumina). Raw sequencing data were processed using 10X Genomics Cell Ranger software (v6.1.1 or v7.0.0).

Of the sorted EGFP<sup>+</sup> cells (Figure 4A), a total of 6,206 cells were captured from DMSO-treated fish, and 6,709 cells were captured from MTZ-treated fish were captured. For AVC cells (Figures 4H and S4H), a total of 9,632 cells were captured from DMSO-treated fish, and 14,173 cells were captured from IWR1-treated fish were captured. Raw data were imported into Seurat v4.3.0<sup>47</sup> to perform quality control, filtering, normalization, integration, clustering analysis, visualization, and identification of DEGs. Scanpy v1.9.3<sup>48</sup> was also used for data visualization. Data sets were trimmed by removing the cells expressing less than 1000 (EGFP<sup>+</sup> cells) or 950 (AVC cells) genes and the genes expressed in less than 3 cells. Cells containing > 45% (EGFP<sup>+</sup> cells) or > 20% (AVC cells) mitochondrial genes and cells containing < 5% ribosomal genes were considered to be of poor quality and were also filtered out. The data were then normalized and logarithmized. Doublets were removed using DoubletFinder v2.0.3.<sup>49</sup> Finally, 4,124 cells (EGFP<sup>+</sup> cells from DMSO samples), 5,230 cells (EGFP<sup>+</sup> cells from MTZ samples), 4,744 cells (AVC cells from DMSO samples), and 3,393 cells (AVC cells from IWR1 samples) were used for further analyses. The merge function of the Seurat package was used to merge objects. Principal component analysis (PCA) was used to reduce the dimensionality of the data, followed by computing the neighborhood graph of cells using the PCA representation. UMAPs were visualized using the Seurat RunUMAP function with the following settings: min.dist = 0.5 and dims = 1:40 (Figures 4B, 4I, and S4A) or 45 (Figures S4I and S4J). Clustering was performed using the FindClusters function with a resolution of 1 (Figure 4B) and 0.5 (Figures 4I and S4I). Clusters regarded as the same cell type were combined using the RenamelDents function. DEGs were identified using the FndAllMarkers and FindMarkers functions with a Wilcoxon rank sum test. For Figure 4J, the CM cluster in Figure 4I was remapped and reclustered, then *cdh5*<sup>+</sup> clusters were removed to analyze only CMs. For Figures 4J and S4E, DEGs were identified using the FndAllMarkers and FindMarkers functions with the following settings: log2FC.threshold = 0.2, min.pct = 0.2, and min.diff.pct = 0.2. GO analysis was performed using enrichR v3.2 with GO Biological Process GeneRIF Predicted Z-score. The Scanpy matrixplot function was used for visualizing the gene expression with matrix plots.

### Quantitative PCR (qPCR)

Total RNA was prepared from sorted EGFP<sup>+</sup> cells using the NucleoSpin XS kit according to the manufacturer's instructions. RNAs were reverse-transcribed with oligo dT primers using Superscript IV (Thermo Fisher Scientific, 18090050). The PCR reaction was performed using KOD SYBR qPCR Mix (TOYOBO, QKD-201) in a CFX Connect thermal cycler (Bio-Rad). The primers used for qPCR were listed in Table S3. The qPCR results were normalized to *eef1a1/1* expression.

## QUANTIFICATION AND STATISTICAL ANALYSIS

### $\beta$ -cat ON CM volume measurement

For the quantification of Figures 2C, 2F, and 2H, the surface of the EGFP<sup>+</sup> region at the AVC was created using the Surface function of the Imaris 10.0.0. The volume of the EGFP<sup>+</sup> region was measured. The measured volume was exported as a CSV file and calculated as a sum.

### CV length measurement

For quantification of Figures 3F, 3I, 4G, S3F, S3K, S3M, and S3P, 105 length was measured by manual tracing using the Imaris 9.8.0, 9.9.1, or 10.0.0 software function Measurement Points. The measured length was exported as a CSV file and calculated as a sum.

### Coverage measurement

For the quantification of Figure S3G, the 2D areas were measured using the ImageJ Polygon selection function. The ventricle area was measured by enclosing the frame of the ventricle with a polygon. The CV-covered area was measured by drawing the polygon with the CV tips as vertices. The percentage of the CV-covered area to the ventricle was found.

### coEC and EdU<sup>+</sup> coEC measurement

For quantification of [Figures S3H](#) and [S3I](#), EdU<sup>+</sup> or DAPI<sup>+</sup> signals were detected using Imaris 10.0.0 software function Spots and filtered spots within the EGFP<sup>+</sup> CV using the Surface function.

### Head length measurement

For quantification of [Figures S2C](#) and [S2E](#), alcian blue-stained larvae were mounted in glycerol. Images were recorded using an SZX16 stereo microscope (Olympus). Head length was measured using CellSens imaging software (Olympus).

### Statistical analysis

Data were analyzed using the statistical function of SciPy and were presented as mean  $\pm$  SEM using the swarmplot function of seaborn.<sup>50</sup> Sample numbers were indicated in the figures. In the dot plots of [Figures 2C](#), [2F](#), [2H](#), [3F](#), [3I](#), [4G](#), [S2C](#), [S2E](#), [S3F–S3I](#), [S3K](#), [S3M](#), and [S3P](#), each dot represents an individual fish. In the dot plot of [Figure S4F](#), each dot represents a sample of endothelial cells sorted from 4–5 fish hearts. [Figures 3F](#) and [S4F](#) shows samples from three independent experiments. [Figures S3F](#) and [S3G](#) show samples from two independent experiments. [Figures 2C](#), [2F](#), [2H](#), [3I](#), [4G](#), [S2C](#), [S2E](#), [S3H](#), [S3I](#), [S3K](#), [S3M](#), and [S3P](#) show samples from one of more than three experiments. Statistical analysis was performed by a 2-tailed Student's *t*-test ([Figures 3F](#), [4G](#), [S2C](#), [S2E](#), [S3F–S3I](#), [S3K](#), [S3M](#), and [S4F](#)), Welch's *t*-test ([Figure S3P](#)), or Mann-Whitney *U* test ([Figures 2C](#), [2F](#), [2H](#), and [3I](#)). Statistical significance was defined as  $p < 0.05$ .